Towards Microfluidic Design Automation

by

Asif Khan

A thesis
presented to the University of Waterloo
in fulfillment of the
thesis requirement for the degree of
Master of Applied Sciences
in
Electrical and Computer Engineering

Waterloo, Ontario, Canada, 2016

I hereby declare that I am the sole author of this thesis. This is a true copy of the thesis, including any required final revisions, as accepted by my examiners.

I understand that my thesis may be made electronically available to the public.

Abstract

Microfluidic chips, lab-on-a-chip devices that have channels transporting liquids instead of wires carrying electrons, have attracted considerable attention recently from the bio-medical industry because of their application in testing assay and large-scale chemical reaction automation. These chips promise dramatic reduction in the cost of large-scale reactions and bio-chemical sensors. Just like in traditional chip design, there is an acute need for automation tools that can assist with design, testing and verification of microfluidics chips. We propose a design methodology and tool to design microfluidic chips based on SMT solvers. The design of these chips is expressed using the language of partial differential equations (PDEs) and non-linear multi-variate polynomials over the reals. We convert such designs into SMT2 format through appropriate approximations, and invoke Z3 and dReal solver on them. Through our experiments we show that using SMT solvers is a not only a viable strategy to address the microfluidics design problem, but likely will be key component of any future development environment.

In addition to analysis of Microfluidic Chip design, we discuss the new area of Microhydraulics; a new technology being developed for the purposes of macking dynamic molds and dies for manufacturing. By contrast, Microhydraulics is more concerned on creating designs that will satisfy the dynamic requirements of manufacturers, as opposed to microfludics which is more concerned about the chemical reactions taking place in a chip. We develop the background of the technology as well as the models required for SMT solvers such as Z3 and dReal to solve them.

Acknowledgements

I would first like to thank Derek Rayside, for his guidance, patience, his knowledge and wisdom, and his trust. For his help in developing all the core ideas in the domain of single-phase microfluidics, multi-phase microfluidics and the strategies used in traversing PDE's using SMT solvers such as dReal. Finally, I would like to thank Derek for his help in reviewing the contents of this thesis, and his help framing it's research in a way to help understand it's true potential.

I would like to thank Vijay Ganesh, for his help, guidance and input, for suggesting the use of dReal as a solver that would enable this line of research as well as allowing me to develop some of the ideas in the single-phase microfluidics section in his ECE 750 class. I would finally like to thank Vijay for his review of the contents of this thesis and his continuous effort and motivation, the research would not be as far along as it is if it weren't for him.

I would like to thank Paul Ward for his review and interest in this area of research.

I would like to thank Thomas Kennedy and Natascha van Lieshout for the work they put in to verifying the microfluidic models used with COMSOL simulations.

I would like to thank Divij Rajkumar for his work in the area of incorporating CEGAR Loops between dReal and Matlab, Stephen Chou for his contribution to the microfluidic diffusion and electrophoretic smt2 models and William Lindsay for his work on error tolerance of PDE's as well as strategies in solving PDE's using dReal.

I would like to thank Murphy Berzish for his work in multi-phase microfluidics, the development of the Manifold tool set, and Atulan Zaman for his help in creating a compiler to generate .smt2 code from microfluidic circuits for the dReal solver.

I would like to thank Ahmed Eltom, Aidan Gallagher, Dhruva Nathan and Sam Jeong for their work in developing and testing the linear actuators used in the PinPress system and Tessa Alexanian, Emily Haggith-Arthur, Logan Money and Ryan Collins for the work they did in creating a control system for the PinPress system.

Dedication

This is dedicated to my parents, no one could ask for anyone better.

Table of Contents

List of Figures

Chapter 1

Introduction

There is great opportunity and need for software-based design automation tools for microfluidics [3]. As compared to the mature and robust industry for software-based design automation tools for digital circuits, which is backed by decades of research, tools for microfluidic design automation are relatively nascent. There has been about a decade of research in the area, and there are relatively few commercial tools.

Microfluidic design is more complex than digital circuit design because of the wider range of physical theories involved, and because of the sensitivity of various parameters. While it is true that both analogue electrical circuits and hydraulic networks can be modelled with some the same mathematics — *i.e.*, voltage is like pressure, whereas current is like flow rate — the channel widths, lengths, and turns in microfluidics have greater impact on their resistances than do wire widths, lengths, and turns in analogue electrical circuits (at least at the scale of the devices under consideration here). So for microfluidic devices, the placement of components and routing of channels is more intimately tied to the functionality of the device.

The current state of practice in microfluidic device design is calculations 'by hand' (perhaps with Matlab) followed by build and test. Building and testing is currently easier and less time-consuming than trying to do a more rigorous design in advance due to lack of appropriate design automation software. As in other engineering fields, this build-and-test approach is limited in terms of size of artifacts that can be designed and the robustness of those artifacts.

This thesis identifies three different kinds of microfluidic devices that could benefit from design automation software: *microhydraulic* (§2), single-phase (§3), multi-phase (§4).

Within each of these domains this thesis identifies and documents some of the analytic equations that would need to be computed by design automation software.

Single-phase and multi-phase are classes of devices that were previously well-known. The idea of microhydraulics is less studied in the literature. The idea of microhydraulics is that the fluid is used to move or maintain mechanical components in position — there is no interesting chemical or biological activity in the device. By contrast, most of the rest of microfluidics is usually concerned with facilitating chemical or biological processes.

The design space of a novel microhydraulic device, the *PinPress*, is described (§2). The PinPress is a programmable die for advanced manufacturing [36]. The PinPress can be quickly reconfigured to form new shapes in a matter of minutes, whereas swapping old-fashioned dies in a production line can take hours.

Furthermore, this thesis investigates the applicability of recent advances in SMT solvers, namely dReal [27], to synthesis of microfluidic device designs. dReal's design intention was as a tool for verifying software or cyber-physical systems. No prior work in the literature proposes using SMT solvers for synthesizing (nor analyzing) microfluidic devices (§1.1). We provide a preliminary evidence that it is feasible to use dReal for microfluidic design synthesis.

Finally, in some circumstances a microfluidic design automation tool might not be able to rely on analytic equations, and might have to use partial differential equations. These are conventionally solved by a finite element analysis. We demonstrate that dReal can perform this analysis for some of the relevant equations (§5.8, §5.9) with coarse meshes §5.7. We also explore novel analytical approximation techniques for the PDEs in question that can be computed more efficiently by dReal (§5.2, §5.3).

This thesis advances towards the goal of microfluidic design synthesis tools, identifying some specific targets and some of the tools and techniques that might take us there. A tremendous amount of work remains to be done — far more than the scope of one masters thesis — before the vision of replicating the digital circuit design toolchain for microfluidics has been fully realized.

1.1 Review of Microfluidic Design Automation Software

1.1.1 Background

Microfluidics chips, lab-on-a-chip devices that have channels transporting liquids instead of wires carrying electrons, are increasingly used in testing assays, drug design and analysis. These chips are already quite complex and their complexity is only increasing rapidly with time [3]. It is all but obvious that designing such chips will require sophisticated software, similar to electronic design automation (EDA) tools used by the microprocessor design industry [8]. Applications for Microfluidic Chips [66] range from STI detection (HIV [35], syphillis [11]), malaria [37], detection of small molecules (ethanol), DNA (viruses) to Proteins such as glycophorin C [65, 67], a protein linked to leukemia.

While design tools for electronic chips largely support bit-vector heavy hardware description languages, microfluidic chip designs are expressed using constraints that span theories such as partial differential equations, and non-linear multi-variate inequalities over the reals. This suggests the use of constraint solvers that are good at solving constraints from many different fragments of mathematics as backends for design tools for microfluidics. Fortunately, SMT solvers are the kind of tools that are good at supporting a variety of different mathematical languages in a seamless way, suggesting a new design methodology for microfluidics chips based on such solvers. Chakrabarty *et alia* describe the overall process of microfluidics design [12, 13].

1.1.2 Current Design Methodology for Microfluidics Circuits

Currently, microfluidics design works by an educated guess-and-check method. Starting from the equations that describe the requirements of the circuit, the microfluidic's engineer guesses design parameters that might work. Then he/she writes, by hand, a Matlab simulation for the circuit. Writing the Matlab simulation requires upwards of four hours, and includes doing some calculations by hand on the side. The Matlab script is typically upwards of 7000 lines, and is usually constructed by modifying a copy of an old script. If the simulation fails, then the microfluidics engineer guesses new values for the design parameters and tries again. In other words, the design process is guess-and-check guided by educated intuition.

To the best of our knowledge Matlab is not able to conduct this design parameter search automatically. First, Matlab is primarily intended as a simulation engine, rather than a

solver. Moreover, Matlab, to our knowledge, does not natively handle systems of non-linear inequalities over the reals: 1. fsolve does not support non-linear; 2. linprog supports inequalities but not non-linear; 3. pdepe dues not support inequalities; 4. fmincon supports non-linear inequalities by a guess-and-check method that we believe is less sophisticated than what is done by modern SMT solvers.

In summary, microfluidic circuit design is, in part, a satisfiability problem over a combination of theories involving ordinary/partial differential equations, non-linear real inequalities, trigonometric functions, and boolean constraints. The current state of practice is that the designer attempts to find valid design parameters by using educated human intuition, and then writes a Matlab script to simulate (verify) that those parameters do indeed satisfy the constraints.

1.1.3 Proposed Solution

Gleichmann *et alia* [28] argue that software should be used to automate this process as much as possible. Here, we present exactly such a methodology for microfluidic chip design based on SMT solvers. We use two powerful solvers for our experiments, dReal [27] and Z3 [19]. Fluid dynamics relies heavily on the Navier-Stokes equation, which is a partial differential equation. In practice, fluid dynamicists usually solve this equation by approximation using the finite different method [51]. Our solver based approach partially realizes Gleichmann's proposal by integrating a number of these steps into one computation.

Our current prototype demonstrates that modern SMT solvers can be used for synthesizing microfluidic circuit designs that are correct by construction. Further work is necessary to make the prototype usable by microfluidic engineers.

1.1.4 Complimentary Works

Following summarizes other strategies that have targeted other challenges in the area of microfluidic chip design. A number of IDE/drawing tools have been developed for microfluidics (*e.g.*, [6, 53]), as well as textual languages (*e.g.*, [41]). McDaniel *et alia* [41] also present a tool for simulating and debugging. This work is complementary to ours: the designer wants both to draw/specify/simulate the circuit and let our system solve for many of the design parameters.

Kahng *et alia* [34] investigate placement methods to minimize the microfluidic chip area.

Once the fluid circuit has been designed, there is a complementary problem of routing electrical control wires for it. This is an NP-hard problem that has been tackled with a graph-colouring heuristic [1].

There has been work similar to what we propose in the context of DNA Assay arrays using Border Minimization Problem Solving techniques [34].

Most recently, work in large scale integration of microfluidic channels are being explored [3, 56].

Araci & Brisk [3] survey the current state of the art in large scale integration of microfluidic circuits. They identify the need for tools like ours, but do not have many to cite. The only tool that they identify that uses any kind of solver is by Minhass *et alia* [44], who use the Gecode (`gecode.org`) constraint programming system to compute the routing, scheduling, and part selection for a microfluidic circuit. The output of our system would be used as the input to their system.

1.2 dReal: A Modern SMT Solver for Reals

In recent years, an open-source tool dReal [27] has been developed to solve nonlinear formulas (polynomials, trignometric functions, exponential functions) over the reals. It is built on opensmt [10] for high level DPLL(T) framework, and realpaver [29] for Interval Constraint Propogation algorithm. It functions by the use of δ-complete decision procedures to determine the truth property of ϕ. δ is the numerical precision defined by the user, and the solver offer a certificate of correctness; a solution when δ-sat or proof of unsatisfiability. δ must be a postive, rational number.

It has been established that the complexity of higher order systems can be combatted by the use of a δ relaxation [26]. This is done by relaxing the system from:

$$\exists x \in I . x > 0 \tag{1.1}$$

to

$$\exists x \in I . x > \delta \tag{1.2}$$

It is concluded that given a δ, a set of first-order sentences can exist where their "truth" property is independent of δ-strengthening. This gives way to the fact that a set of

first-order sentences that return "unsatisfiable" is in fact unsatisfiable, regardless of the δ-precision of the system, and this system is known to be δ-robust.

It is proven once a numerical method has proven that it can be solved using a particular numerical method, it is then suitable for solving using δ-decidability [26].

The δ-completeness of a system can be determined by varying the size of δ in order to determine the sensitivity of the δ-robustness of the system [25]. A system is said to be unsafe, if the satisfiability of the system is dependent on the precision of δ.

An alternatie solving method for nonlinear functions is Cylindrical Decomposition [15], however it relies on a symbolic approach that is restricted to polynomial constraints. Numerical methods used in solving nonlinear functions range from optimzation algorithms [46], interval-based algorithms [24], Bernstein polynomials [45] and linearization algorithms [23]. dReal uses a combination of numerical and symbolic algorithms, accepting formulas in standard SMT-LIB 2.0 format allowing it to solve sin, tan, arcsin, arctan, exp, log, pow, and sinh. Information on variables are declared using atomic formulas and the precision of delta can be set via (set-info :precision 0.0001). This is useful for engineering applications, especially where many solutions exist. Bounded model checks are performed by incorporating safety properties to the SMT formula.

1.2.1 Solvers

Uses a base DPLL(T) [10] framework, where an Interval Constraint Propogation (ICP) [29] solver is used to check if a set of theory of atoms is consistent. ICP works by using a "branch-and-prune method", where the interval is divided into sub interval, and each subinterval is explored. A check and assert method uses the ICP solver to contract the interval assignments on defined variables, and eliminate domains that do not contain any solutions. Backtracking and Learning method keeps a stack of mappings from variables to unions of intervals. When a conflict is reached, the solver backtracks to the previous environment and collects constraints that led to the conflict. These subset of constraints are turned into a learned clause and added to the original formula. Witness for δ-Satisfiability is the ground formula of the original formula given δ relaxation of the formula. Proofs of Unsatisfiability is a proof tree that be can be verified by testing the negation of the formula.

1.3 Research Impact

There are not yet any academic publications as a result of this thesis work. There are, however, other external results.

The PinPress work is the subject of a patent [36] and an associated startup company, Maieutic Enterprises Inc.[1] This company has won a number of grants and awards, including:

- AC Jumpstart — CAD$60k
- OCE VIP1 + TalentEdge — CAD$30k
- Futurpreneur — CAD$15k
- LESI Global Award[2] — USD$31.5k
- HAX Accelerator — USD$25k
- 'Get in the Ring' Kauffman Foundation — USD$5k

This thesis work has also sparked two NSERC Discovery proposals from University of Waterloo faculty (one successful; the other currently under review).

During the course of this thesis work, a number of under-graduate co-op, capstone design projects and 499 students were supervised, some of whose work is incorporated into this document (with citation):

1. Thomas Kennedy (4B Nanotechnology Engineering)
2. Natascha van Lieshout (4B Nanotechnology Engineering)
3. Christopher Willar (1B Nano Engineering)
4. Divij Rajkumar (4B Computer Engineering)
5. Stephen Chou (4B Computer Engineering)
6. William Lindsay (4B Computer Engineering)
7. Murphy Berzish (4A Software Engineering)
8. Ming-Cee Yee (2B Computer Science)
9. Ahmed Eltom (4A+B Nanotechnology Engineering)
10. Aidan Gallagher (4A+B Nanotechnology Engineering)
11. Dhruva Nathan (4A+B Nanotechnology Engineering)
12. Sam Jeong (4A+B Nanotechnology Engineering)
13. Tessa Alexanian (4A+B Systems Design Engineering)

[1] http://maiuetic.ca

[2] https://www.lesi.org/about/lesi-news-and-updates/2015/05/28/les-foundation-graduate-student-business-plan-competition-awards-international-global-prize-to-studer

14. Emily Haggith-Arthur (4A+B Systems Design Engineering)
15. Logan Money (4A+B Systems Design Engineering)
16. Ryan Collins (4A+B Systems Design Engineering)

Additionally, there are two other masters students currently working on projects initiated by this work.

Finally, some of our models have been used to improve both the performance[3] and correctness of dReal.[4]

[3]Soonho Kong, personal communication regarding dReal v3.15.10.01, October 6, 2015. https://github.com/dreal/dreal3/tree/master/benchmarks/smt2/microfluidics

[4]dReal3 issue #150, August 2015, https://github.com/dreal/dreal3/issues/150

Chapter 2

Microhydraulic PinPress

We introduce the term microhydraulics to distinguish the work from microfluidics. In microfluidics the fluid in the circuit is of interest, whereas in microhydraulics the fluid is just a means to secure solid parts. Microfluidic circuits might be concerned with medical diagnostics ("lab on chip"), chemical synthesis, or other applications where some property of the fluid is either unknown or intended to change. Microfluidic circuits typically do not have solid moving parts, whereas microhydraulic circuits do.

This following are the elements necessary in developing the PinPress solution:

1. Comparison of actuators (§2.4). Five different kinds of actuators for potential use in microhydraulics are analyzed and compared. Homopolar (linear) motor is selected as the best choice for the PinPress due to the density of the device.

2. Controls. A method to address each individual motor is described, analagous to an active AMOLED system (§2.5.1).

3. Locking mechanisms. A two-stage physical locking mechanism for securing the pins into position. The primary locking mechanism is fluid-based §2.6.1. The secondary is gel-based §2.6.2.

4. Software models. A model used to describe aspects of reconfigurable tooling that can be used to reason around using an SMT-solver such as dReal (§2.7).

5. Physical prototypes. Iterations in the development of the first microhydraulic system is documented (§2.8).

2.0.1 Motivation

Dies used in high-volume manufacturing degrade with use over time. When a die degrades beyond acceptable tolerances the production line must be stopped and that die repaired or replaced. The longer the production line is stopped, the more expensive the stoppage is. An ideal tool would be an infinitely customizable die with a programmable surface, comprised of hundreds or thousands of tiny pins that are held in place by a non-compressible fluid. These programmable dies can then easily change shape to produce different kinds of items allowing for compensation for wear and tear, reduced changeover time and customization to individual consumer needs. When a conventional die degrades it is difficult and time consuming both to diagnose exactly where the problem is and to repair it. The programmable die, by contrast, can self-diagnose where it is out of tolerance and automatically return itself to the correct, desired shape. Mechanical wear on the programmable die is experienced by each individual pin. The die can measure the length of each pin individually by measuring its electrical resistance. This measurement is compared to the desired length of the pin to detect which pins have been worn down. Then, using microhydraulics, it can extend pins that have been worn down so that the die returns to the desired shape. Note that we do not currently expect this die re-calibration process to occur while the production line is running: the line will still have to be stopped, but for a much shorter period of time than is currently the case.

It is believed that these programmable dies are widely applicable in high-volume manufacturing, but initial focus is on softer materials such as plastic extrusion. Alternatively, a programmable surface can be used to allow for mass-customization. For instance, though most consumers have feet that fall into the standard predefined industry standards, they often do not take into consideration the dimensions of the foot and leads to the need for consumers to try multiple shoes on, looking for a shoe that both matches the style preferences and foot dimensions. With the programmable surface, these trade-offs can be avoided by adjusting the shape of the shoe to match the shape of the feet of the consumer, enabling customization at high volumes.

High-volume manufacturing equipment is, in contrast to the items it produces, typically specialized and customized for each installation. Consequently, each programmable die produced will also need to be customized for its intended deployment context. Each programmable die could have different pin diameter, pin length, different number of pins, different pin materials, etc. Similarly, the microhydraulic system controlling the pins might be designed with different fluid (e.g., water, inorganic oil, organic oil, etc) depending on the temperature and other factors of the deployment environment.

Designing one of these programmable microhydraulic tools involves many variables with

complex inter-relationships. Performing the calculations "by hand" with a tool like Matlab can take weeks of guess-and-check computations for someone with extensive background training in materials and microfluidics. Reducing die design time and the skills required of the die designer makes such an endeavor more practical. A system in which someone lacking deep theoretical knowledge of materials and fluid dynamics could design a die in a few hours using standard design rules would be a significant improvement in design time.

Matlab is essentially a calculator: it propagates concrete input values through some formulas to produce concrete output values. It does not (primarily) solve systems of equations, where solving a system of equations means searching for values of the variables that give the equations a desired output. For example, what values of x make $f(x)$ evaluate to zero? SAT solvers are software tools that solve systems of boolean equations. SAT stands for the boolean satisfiability problem. A boolean equation is one in which all of the variables are either true or false. SAT solvers have been an active area of research for over fifty years, and have seen tremendous progress in the last twenty years. They are routinely used in the design of both computer hardware and software, for verification and synthesis tasks.

SMT solvers are recent extensions of SAT solvers. SMT stands for *SATisfiability Modulo Theories*. Different SMT solvers add different kinds of functionality to a SAT solver. For example, there are a number of SMT solvers that support integer-valued variables, or variables of array type, or bitvector variables. These kinds of variables are all useful in computer hardware and software. In the last three years researchers at Carnegie Melon University in Pittsburgh have designed a SAT solver called dReal that also works with real-valued variables. However, using dReal directly would still require the designer to have deep knowledge of materials and fluidics, because the designer would still need to know what equations appropriately characterize the die to be designed. The equations that are relevant change as the sizes and materials change. What the industry needs is a high-level hardware description language for die design, with an associated mechanical translation system and computational engine (dReal). The outputs of the computational engine must also be translated back into terms of the high-level design, and the final design should be used to produced a Matlab script or COMSOL model that can simulate the design as an extra verification step. VHDL and Verilog are the two most common high-level hardware description languages for digital computer design. VHDL is the language in common use at the University of Waterloo. Therefore, we propose to design a hardware description language inspired by VHDL but suitable for microhydraulics. Rayside's research group at the University of Waterloo already have a framework that is suitable for quickly developing and implementing such languages.

Unlike multiphase and singlephase microfluidics, microhydraulics is in itself a new field.

As such the following chapter provides a summary of the new technology, how it functions and the design consideration that need to be made. Using this knowledge, future resesarch will be conducted on developing software models that fully describes these system, as well as implementation of using a solver such as dReal to explore the design space for various environments and applications.

2.0.2 Innovation

A novel hardware description language has been designed and implemented for microhydraulic circuits, called Manifold. Users of Manifold will specify the known parameters of their circuits, and an SMT-based engine (dReal) will compute the values for the other parameters that satisfy the design objectives and physical constraints. This language and its associated toolset allows users who have relatively limited knowledge of microfluidics and materials to design complete microhydraulic circuits. It will also significantly reduce the time an expert needs to design such a circuit, and reduce the opportunities for error. Industry needs this technology because every programmable die that is created must be a custom design, tailored to the specific manufacturing context in which it is to be used. Our research group has already developed an extensible framework for hardware description languages. This framework makes it relatively easy to define new hardware description languages in terms of the components they consider, the connections they have, and the translations associated with same. So a certain amount of software infrastructure is already in place. Previously we have used this framework primarily for translating one description language for digital computer hardware to another such language, but our preliminary exploration of microhydraulics suggests that it is well within the capabilities of the framework. The plan is to tackle the potential inaccuracies of dReal's output in three ways. First, by building safety factors into the design constraints we can search for solutions that have some variance when compared to the actual problem. Second, preliminary experiments suggest that we can set dReal's delta value below the threshold tolerance of the manufacturing process, so that inaccuracies would not matter in production. Third, as a verification step we will have our system automatically produce a Matlab script or COMSOL/Modelica model(s) to simulate the circuit given the design parameters computed by dReal, to verify that the synthesized circuit design does indeed perform as expected. If the results are not validated through the verification method given some tolerance, the system will learn from the model using a method known as Counter-Example Guided Abstraction Refinement to add the gained knowledge to the model and regenerate new solutions.

Figure 2.1: Actuators at different heights [36]

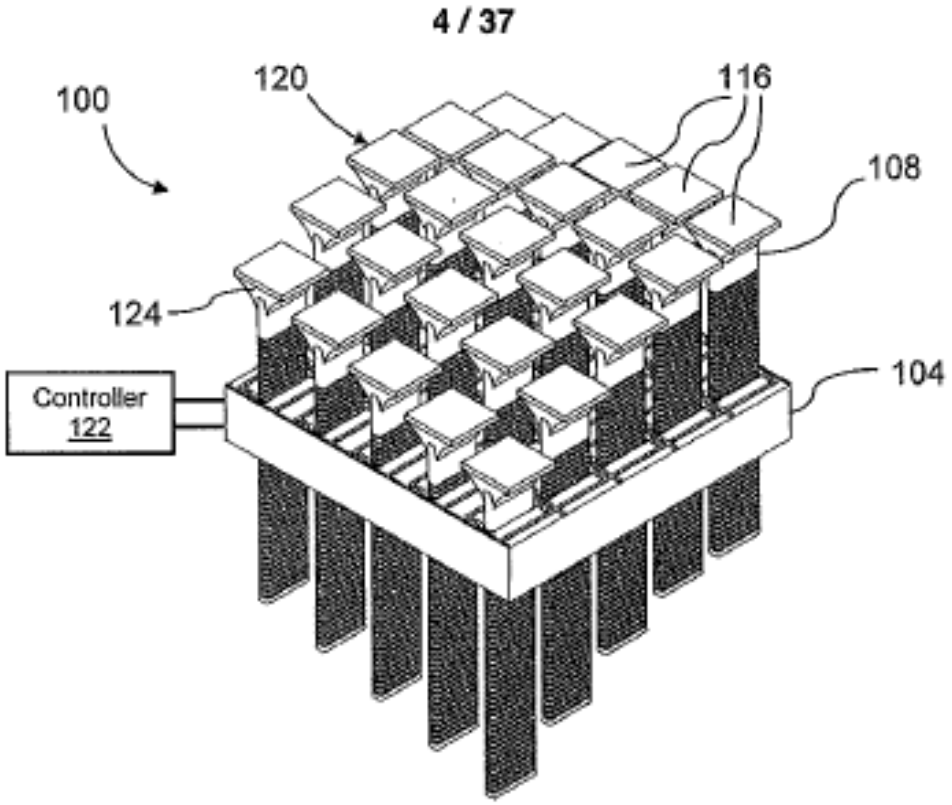

2.1 Functionality of PinPress

Here we describe an electronically controllable surface who's physical topology can be adjusted and dynamically assume a variety of persistent shape. The targeted application is manufacturing; allowing for the realization of reconfigurable tooling. Tools that can be adjusted in line to allow for in-line manufacturing corrections and mass customization. This is how the current design on the system works.

The surface is discretized into tiny actuators (pins), that can be actuated by the use of Lorrentz Force. By actuating the pin up and down, we transform the topology of the system as seen in figure 2.1.

The system then holds the pins temporarily in place by the use of a gel-based clamp,

figure 2.13, and liquid is filled in the chamber as seen in figure 2.12. Once the pins are in place, and fluid has filled the chambers, the cavities are capped allowing for force to be placed on top to surface of the system [36].

2.2 Potential Applications in Manufacturing

2.2.1 Metal Bending

The idea of using reconfigurable tools for bending sheet metal has been properly documented in [31]. Here, hydraulic actuators are used to reconfigure the press to create different types of curves for manufacturing. By adjusting both the horizontal and vertical shape of the press, the sheet metal is bent into different curvatures for applications such as in aerospace and construction.

Figure 2.2: Reconfigurable Discrete Die used for metal bending [48]

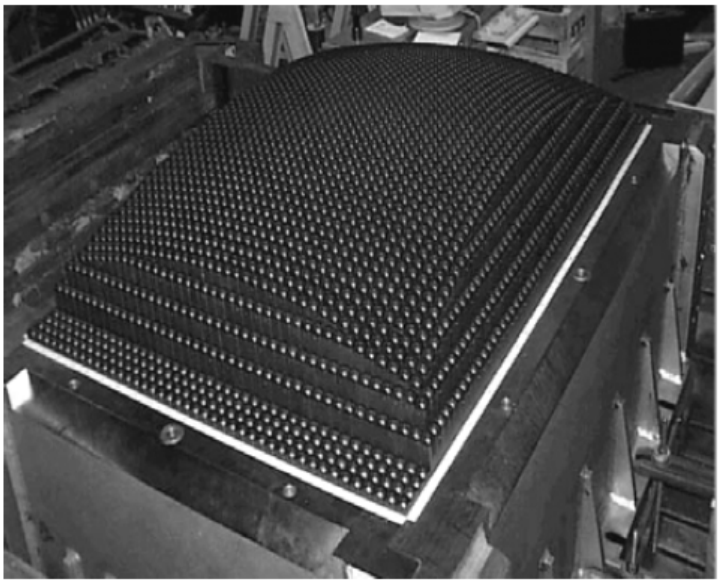

Figure 2.3: How reconfigurable vacuum forming tool would work [59]

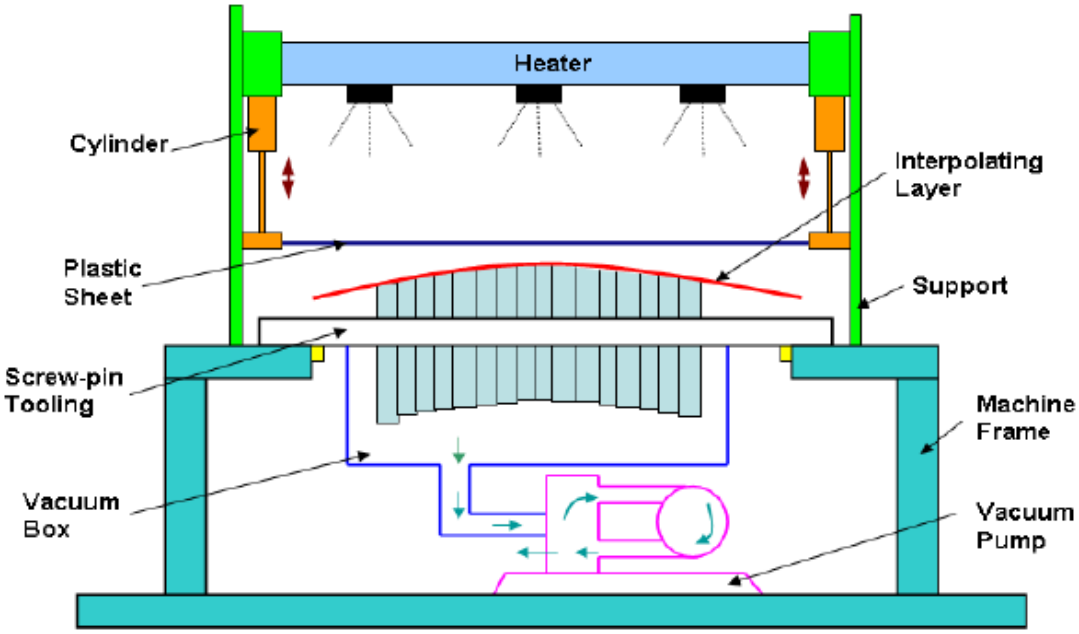

2.2.2 Vacuum Forming

Vacuum forming or thermoforming is done by heating a deformable material and shaping it over a mold by the use of a vacuum [59]. Process is as follows; a material is clamped over the mold of interest and heated. Once the material is malleable enough, a vacuum is introduced from underneath the mold which causes the thermo form material to take the shape of the mold. Finally, the material is cooled and hardens in its new shape. A reconfigurable vacuum tool is realized by replacing the mold with an array of linear actuators.

Due to natural limitations in vacuum forming, the forming process is limited to the shape of the surface. This lends nicely to using an array of linear actuators as the technology is limited to only making surface adjustments and suggests that a programmable surface would work nicely with vacuum forming technology.

Figure 2.4: An example slit die extruder. The edges can be modified with reconfigurability. [4]

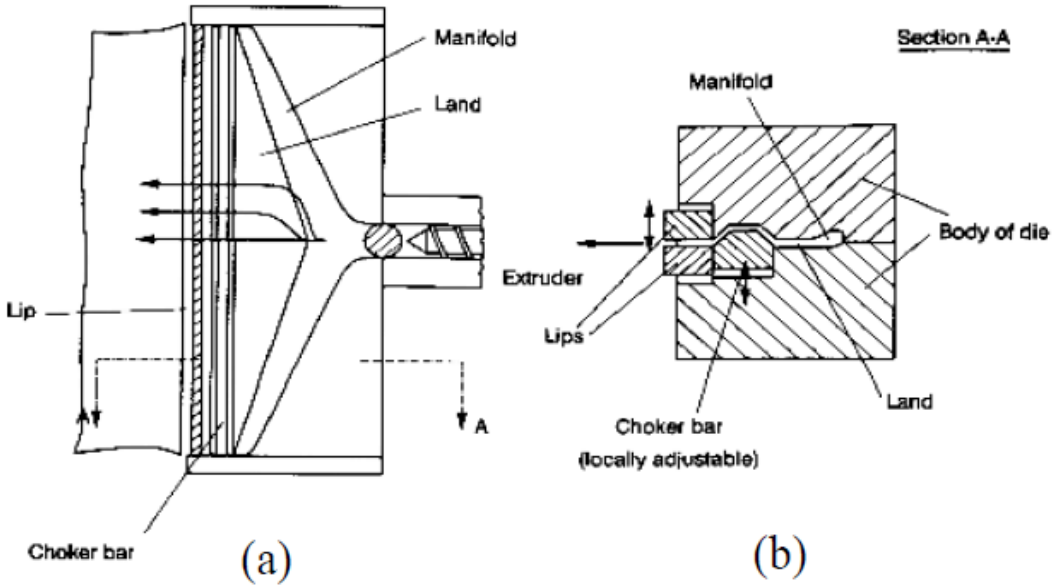

2.2.3 Slit-Die Extrusion

Die extrusion is often used to for processes where only the two dimensional profile of the system matters [4]. The die acts as a nozzle that then funnels the material into a desired shape which is then extruded out. Often this method is used on materials such as aluminum, or softer materials such as polyurethane.

Alternatively, the die can be composed of a line of linear actuators, acting as a ”smart nozzle”, allowing for adjustments to the shape and thickness of the material being extruded. Such as system would allow for adjustments in-run; requiring the manufacturing line to experience less downtime.

Figure 2.5: Reconfigurable Discrete Die method used for Tubular Formation [2]

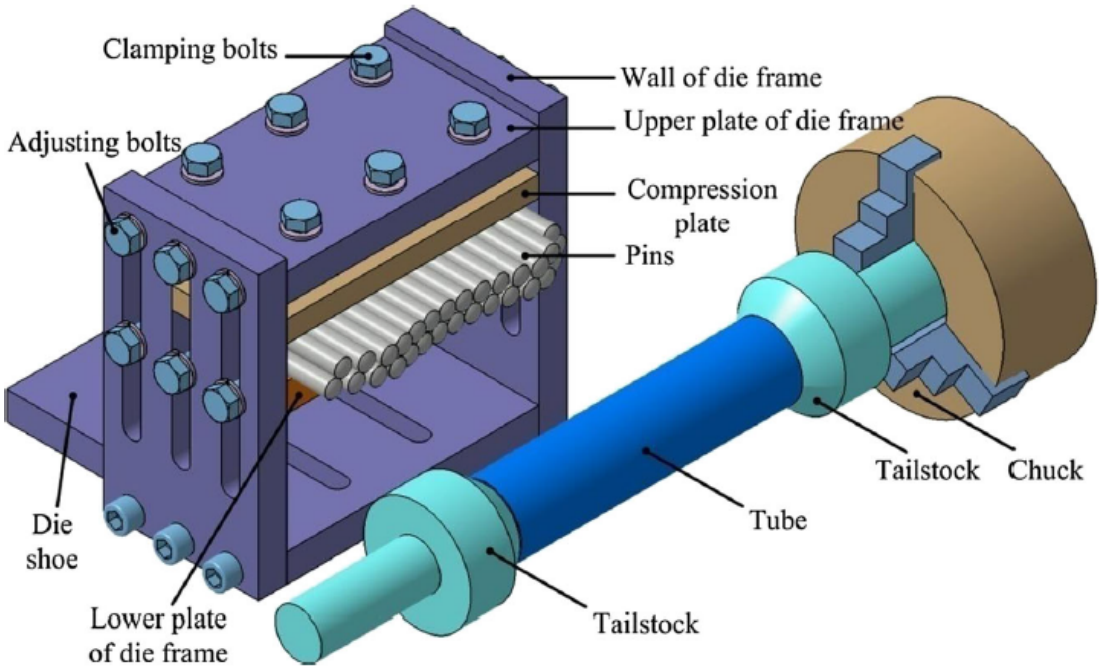

2.2.4 Discrete Die for Tubular Formation

The application of using a reconfigurable tool for use in making tubular parts has been demonstrated in [2]. Similar to die extrusion, the shape of a single line is adjusted to various desired profiles. Once adjusted to the desired profile, the part that is being formed is rotated in place. As the die rubs against the part being formed, it shapes the part into the desired tubular structure.

2.3 Design Goals

For our first working prototype, the followings considerations are made:

1. Pin Design: the pin needs to be designed in a manner that maximizes velocity while minimizing it's weight. This means that the pin needs to be made of a low density material with conductive traces that have high current-density to mass-density ratio, such as aluminum.

2. Strong Magnetic Field: the magnetic field in the system must be aligned, strong and perpendicular to both the direction of motion as well as the direction of current. In our design the field is produced by permanent magnetics (N42 - N52) with approximately one Tesla of strength. In order to reduce strain in the system, magnets that are abreast to one-another have opposite magnetic fields. Current in each field run opposite to one-another to produce motion parallel to each other. It should be noted that magnetic fields decay rapidly and this decay needs to be accounted for in the design.

3. Wiring: Since the amount of current required in the system is significant (>5A), we need to use wires that can handle the large amount of current in question.

4. Maintain Electrical Contacts: In order to allow for motion, the contacts used to transfer current into the pin must be perfectly flat and aligned in order to ensure smooth and consistent motion. Also, a force needs to applied between the pin and the electrical contact in order to reduce the resistance between the contact and the pin. When the pin is moving in the horizontal plane, this does not pose an issue as gravity provides the force necessary in order ensure electrical contact. However, when the pin moves in the vertical direction, gravity does not provide the force necessary in order to ensure electrical contact, and therefore another source needs to be investigated in order to create this force such as material elasticity or magnetic ink. Material elasticity refers to using a material in place of a spring in order to ensure electrical contact (because a spring cannot be miniaturized to this level). A soft magnetic ink may provide the force necessary for this application, however, the magnetic field produced by the permanent magnets is not equally strong across the surface of the magnet, which causes the magnetic ink to also act as an opposing force to motion (encourse the pin to stay in the middle of the magnet, rather than move up or down).

5. Feedback Mechanism: a mechanism needs to be used to determine the location of the pin. This can be one of many options including the use of a variable resistor, use of a capacitor who's area varies with pin movement or a magnetoresistor.

6. Friction: Lower friction reduces the amount of force required for pin motion, while also ensuring electrical contact for a longer period of time. Smooth surface also reduces sparking and resistance inherent in the linear motor.

We will be looking for ways to improve our design through:

1. Increase Pin Density: This can be achieved through use of smaller magnets, or through the production of a customized magnetic shape.

2. Increase Pin Strength: This can be done using new designs structures to better distribute the force at the tip of the pin and by using stronger materials such as a titanium derivative.

3. Increase Actuation Force: We can increase the force of linear actuation by enhancing the effect of Lorentz Force in the system. This can be done by using a stronger magnetic field (external magnetic field, better permanent magnets), increase the amount of current that is passing through the system (using better materials, circuit components) and increasing the path the current runs through in the magnetic field.

4. Control system: use of a sensor to determine the location of the pin. Sensors based on magnetic principles (such as eddy currents, magnetoresistance) prove to be difficult in our system as they are effected by the magnetic field used for actuation. This leaves to explorable solutions; a) a variable resistance strip or b) a capacitive sensor. The variable sensor works by increasing the travel distance a current needs to pass through a resistor as the pin moves. The increase in resistance can be then attributed to the position of the pin. The capacitive sensor works by using a capacitive plate, who decreases in area as the pin moves. The reduction in area, results in a reduced capacitive value of the sensor which in turn can be attributed to the position of the pin. The limitation of a variable resistor is that it requires a significant amount of force to be applied on the surface to ensure electrical contact, and the limitation of a capacitive sensor is the distance between teh two capactive plates must be kept constant at all times. A small change in the distance between capacitive plates would effect the capacitance value of the capacitor as equally as the change in the area of the capacitor. This can be seen through the capacitance equation:

$$C = \frac{\varepsilon_0 \varepsilon_r A}{d} \tag{2.1}$$

2.3.1 Terminology

A survey into prior art was completed by [58], identifying key terms needed to evaluate various technological methods for reconfigurable pin type tooling.

1. *Pin Density:* this term is used to identify whether the pin design uses a close-packed solution or a uniformly space solution. This term can also be used to define the number of individual pins can be actuated per unit area.

2. *Pin Actuation Methods:* This is used to describe specific technological strategy used such as lead-screw driven or in the case of our research, rail motor actuation.

3. *Pin Position Control Method:* Specifically, this term is used to differentiate the difference between manually adjusted pin control versus electronic, computer-enabled systems. A distinction can also be made between user-driven design adjustments, versus an automatic, sensor-based algorithmically driven design adjustments.

4. *Tool Surface Smoothing Method:* Since a pin type solution will inherently result in a dimpled surface, this term determines the method used for prevent these dimples. These methods include but are not limited to a deformable interpolating layer above the pins, deformable pin tips, and covering the surface with a harden-able material.

5. *Degrees of Freedom:* a 2-D solution is defined as a row of pins; a 3-D is a surface of pins that can be varied in height and a 4-D solution is a solution who's surface can be varied in time.

6. *Tool Use:* a direct tool use solution is one that directly shapes the final product while an indirect tool use solution is one that makes an intermediate structure which is then used to shape the final product (such as sand casting).

2.3.2 Comparison of Reconfigurable Pin Type Tooling

The above figures is a summary of patents and prototypes in the domain of reconfigurable pin type tooling, their technological strategies and an evaluation of the solutions performance on various criteria. Figure 2.8 below shows a general trend of technological improvement in the field.

Figure 2.6: Various patents in the domain [58]

Patents			Reconfigurable Tool Taxonomy						Ranking of Characteristics 1 = Bad, 5 = Good								
			T1	T2	T3	T4	T5	T6	R1	R2	R3	R4	R5	R6	R7	R8	R9
			Pin Density [1]	Pin Actuation Method [2]	Pin Position Control Method [3]	Tooling Surface Smoothing Method [4]	Degrees of Freedom [5]	Tool Use [6]	High Surface Resolution (char #1)	Smooth Forming Surface (char #2)	Rapid Reconfiguration (char #3)	Individual Pos and Vel Control (char #4)	Easily Configured for Manufacturing (char #5)	Withstands High Forming Loads (char #6)	Wide Range of Temperatures (char #7)	Allows Vacuum to be Drawn (char #8)	Portable and Lightweight (char #9)
Ref. Name	Year	Ref. #															
Cochrane	1863	11	C	M	Ma	PT	3-D	D	3	2	2		3	4	5	1	1
Ansted	1892	12	C	M	Ma	PT	2-D	D	3	2	1		1	3	4	1	2
Elkins	1920	13	C	M	Ma	PT	2-D	D	3	3	2		1	2	4	1	2
Williams	1923	14	U	M	Ma	PT	2-D	D	2	2	2		2	2	4	1	3
Tegarden	1957	15	C	M	Ma	PT	2-D	D	3	3	1		1	1	4	1	2
Hess	1931	25	C	M	Ma	PT	3-D	D	4	1	4		3	1	2	3	3
Trudell	1942	26	C	M	Ma	DP	3-D	I	1	4	2		3	2	2	2	3
Walters	1943	18	U	M	Ma	ILA	3-D	D	2	4	2		3	2	4	1	2
Wakefield	1943	42	C	M	Ma	PT	3-D	D	4	1	1		2	5	5	3	2
O'Kelley	1945	17	U	M	Ma	DP	2-D	D	1	2	3		2	1	2	1	3
Hicks	1961	43	C	M	Ma	PT	3-D	D	5	2	1		3	5	4	3	5
Humphrey	1971	27	C	M	Ma	ILD	3-D	D,I	4	4	3		4	2	2	5	4
Whitacre	1971	44	C	RNC	AS	PT	3-D	D	4	4	2	1	3	5	5	3	3
Pinson	1980	19	U	M	AP	PT	4-D	D	2	2	4	4	3	2	3	2	2
Fuchs	1982	20	U	H	Ma	PT	3-D	D	1	4	3		2	1	2	4	4
Morita	1993	16	C	M	AP	PT	2-D	D	3	2	4	4	2	4	3	1	2
Kommineni	1988	21	U	M	Ma	PT	3-D	D	2	1	2		2	2	2	4	5
Hoffman	1998	24	U	RNC	AS	DP	3-D	D	2	4	3	3	2	1	2	4	2
Bernardon	1992	28	C			ILD	3-D	D	4	4			2	1	3	4	2
Hoffman	1992	29	C	M	Ma	ILD	3-D	I	5	4	4		3	2	3	1	4
Umetsu	1993	30	C	M	AS	PT	3-D	D	4	1	3	2	3	2	4	3	2
Todoroki	1993	45	C	RNC	AS	PT	3-D	I	3	2	2	2	2	2	4	2	2
Hong	1994	46	C	M	Ma	PT	3-D	I	4	2	4		3	1	2	3	3
Berteau	1994	39	C	M	AS	ILD	3-D	D	4	4	3	4	3	4	3	4	3
Schroeder	1998	41	C	M	AS	CHL	3-D	D	4	4	3	2	4	4	4	2	2
Laskowski	1998	47	U	M	AS	PT	3-D	D	2	1	3	3	2	2	3	3	3
Haas	1996	31	C	M	AP	ILD	3-D	D	3	4	3	3	4	4	3	3	1
Sullivan	2000	32	C	M	AP	ILD	4-D	D	3	4	5	5	4	4	3	3	1
Nardiello	2000	33	C	M	Ma	ILD	3-D	D	3	4	2		4	5	5	3	2
Haas	2000	34	C	M	AP	ILD	3-D	D	3	4	3	3	4	4	3	3	1
Papazian	2001	35	C	M	AP	DP	3-D	D	3	4	3	3	4	4	3	3	1
Papazian	2002	36	C	P,H	AS	ILD	2-D	D	2	4	4	3	1	4	3	1	2
Meilunas	2002	37	C			ILD	3-D	D	3	4					3	5	
Haas	2003	38	C	M	AP	PT	3-D	D	3	2	3	3	4	4	3	3	1
Shemill	2004	23	U	M	Ma	ILA	3-D	D	2	4	2		3	2	3	5	3

1) **C** = Closed Packed Matrix and **U** = Uniformly Spaced
2) Actuation Method = Moving Pin Up and Down. **P** = Pneumatic, **H** = Hydraulic, **M** = Mechanical, **RNC** = Robot or Numerical Control
3) **Ma** = Manual, **AP** = Automatic Parallel, and **AS** = Automatic Serial. **Automatic implies computor controlled**
4) **ILD** = Interpolating Layer Detached, **ILA** = Interpolating Layer Attached, **DP** = Deformable Pin Tips, **CHL** = Covered with Hardenable Layer, and **PT** = Pins Themselves.
5) **2-D** = (x,y), **3-D** = (x,y,z), and **4-D** = (x,y,z,time)
6) **D** = Direct and **I** = Indirect

Figure 2.7: Various types of Reconfigurable Tools [58]

			Reconfigurable Tool Taxonomy									Ranking of Characteristics 1 = Bad, 5 = Good					
Reduction to Practice			T1 Pin Density[1]	T2 Pin Actuation Method[2]	T3 Pin Position Control Method[3]	T4 Tooling Surface Smoothing Method[4]	T5 Degrees of Freedom[5]	T6 Tool Use[6]	R1 High Surface Resolution (char #1)	R2 Smooth Forming Surface (char #2)	R3 Rapid Reconfiguration (char #3)	R4 Individual Pos and Vel Control(char #4)[7]	R5 Easily Configured for Manufacturing(char #5)	R6 Withstands High Forming Loads (char #6)	R7 Wide Range of Temperatures (char #7)	R8 Allows Vacuum to be Drawn (char #8)	R9 Portable and Lightweight (char #9)
Nakajima	1969	48	C	RNC	AS	ILD	3-D	D	5	4	2	2	4	2	3	4	3
Wolak	1973	49	U	M	Ma	ILD	3-D	I	3	4	2		3	3	3	5	2
Wright	1981	50	C	M	AS	PT	3-D	D	2	1	3	2	3	2	3	1	3
Hardt	1980-92	4,52-57	C	M	AS	ILD	3-D	D	4	3	3	3	4	4	3	3	1
Kleepsies	1998	5	U	M	AS	ILD	3-D	D	1	3	3	3	3	2	3	5	3
Walczyk	1998	60	C	H	AP	ILD	3-D	D	3	4	3	3	3	4	3	3	1
Walczyk	1998	58	C	M	Ma	ILD	3-D	D	5	4	2	2	4	4	3	3	2
Finckenstein	1991	6	C	RNC	AS	ILD	3-D	D	4	3	3	3	3	3	3	3	2
Eigen	1992	7	C	M	AP	CHL	3-D	D	4	4	3	4	4	3	3	3	2
Papazian	2002	63	C	M	AP	ILD	4-D	D	3	4	5	5	4	4	3	3	1
Walczyk	2003	8	C	M	AP	ILD	4-D	D	3	4	5	5	4	4	3	5	1
Prabhakara	2002	9	C	M	AP	ILD	4-D	D	3	4	5	5	4	4	3	5	1
Munro	2004	10	C	M	AP	ILD	4-D	D	3	4	5	5	4	4	3	5	1
Haas	2002	67	C	M	AP	ILD	4-D	D	3	4	4	4	4	4	3	3	1
Boas	1997	68	C	M	AS	ILD	3-D	D	3	4	3	3	4	4	3	4	2

1) **C** = Closed Packed Matrix and **U** = Uniformily Spaced
2) Actuation Method = Moving Pin Up and Down. **P** = Pneumatic, **H** = Hydraulic, **M** = Mechanical, **RNC** = Robot or Numerical Control
3) **Ma** = Manual, **AP** = Automatic Parallel, and **AS** = Automatic Serial. **Automatic implies computor controlled**
4) **ILD** = Interpolating Layer Detached, **ILA** = Interpolating Layer Attached, **DP** = Deformable Pin Tips, **CHL** = Covered with Hardenable Layer, and **PT** = Pins Themselves.
5) **2-D** = (x,y), **3-D** = (x,y,z), and **4-D** = (x,y,z,time)
6) **D** = Direct and **I** = Indirect

Figure 2.8: Technology Trend in Reconfigurable Tools [58]

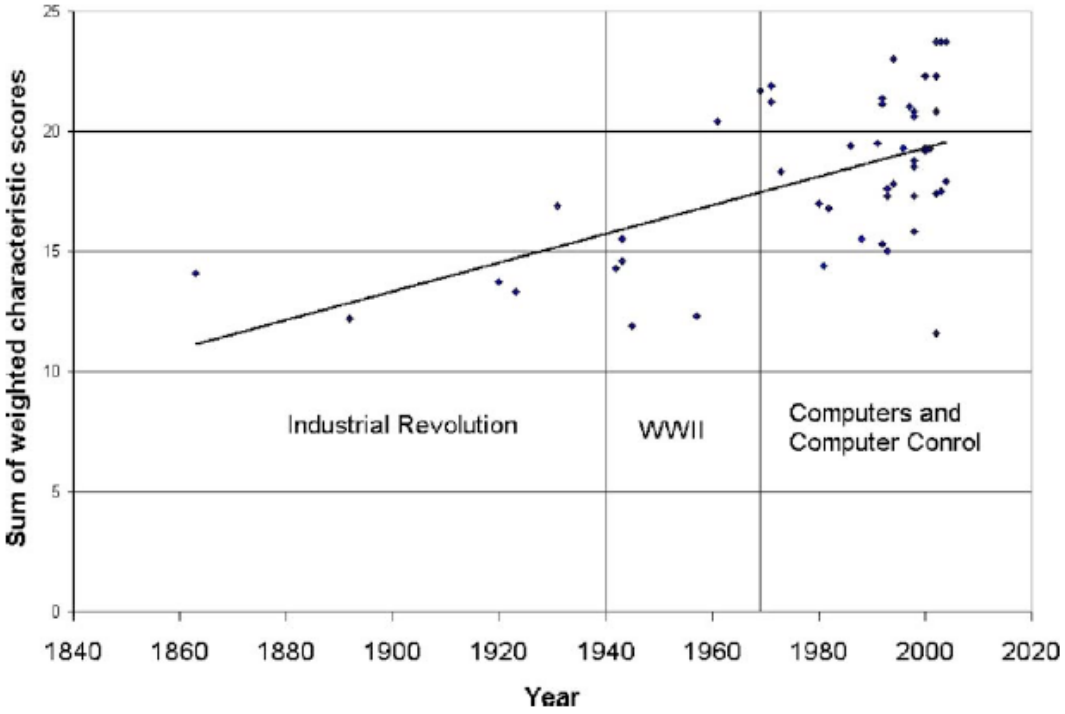

2.4 Comparison of Actuators

An initial investigation in existing linear actuation methods was conducted in order to see if a) an existing solution already existed or if b) there existed a technology that would suit our purposes but had not yet been applied into this domain. Typically, a linear motor create linear motion, rather than a rotational motion typically found in electric motors.

2.4.1 Mechanical Actuators

These motors operate by converting rotational motion into linear motion. There are three types, screw, wheel and axel and cam. They are manually operated, cheap and repeatable. Though these actuators have relatively accurate step size, it suffers from a few shortcomings that do not make it ideal for use in a programmable surface.

First of all, the mechanical components in any mechanical device tends to weaker, and buckle easily under pressure as they are reduced in size due to there being less material to dampen stress and strains being applied to the system [54]. Second, mechanical motors tend to be unnecessarily bulky simply because there is a need for a section which converts the rotational motion of the motor into a linear motion. This conversion component (the nut) puts a limit to how small the footprint of the motor can be. Another limitation is that the speed and accuracy of the motor is limited to the size of the nut. This limitation is the reason that smaller mechanical actuators are typically slower than larger ones [54]. Finally, since there are no electrical components, it is difficult to control such a system via a computer.

2.4.2 Electro-mechanical Motor

Electro-mechanical motors are similar to mechanical motor, except that the nut used to control the actuator is replaced by an electric motor. These actuators tend to be cheap, repeatable and automated as these can be controlled by a DC motor, and can include a feedback mechanism; either a variable resistor or a capacitive sensor. Along with sharing many of the same limitations as it's mechanical brethren, it has many more moving parts than a mechanical actuator, which are more prone to wear.

2.4.3 Hydraulic and Pneumatic Actuators

A hydraulic solution for a programmable surface targeted towards manufacturers seems plausible at first. Using a incompressible fluid such as water, the hydraulic fluid would in fact be strong to take on the forces found in manufacturing. However, the weakness in a standard hydraulic design is in fact found in valve. The strongest sub-cm^3 valve found has had a maximum pressure of 1.3 MPa before leaking [47].

Another problem with using a hydraulic-type design in making a programmable surface is the need for an array of micro-pumps. This proves to be a design challenge as they can have a substantial foot print and have not shown to produce pressures greater than 5 MPa [7]. The maximum output of a micropump can prove to be a limiting factor since the hydraulic resistance, which for a cylinder is given by the equation:

$$R_h = \frac{8\mu L}{\pi R^4} \tag{2.2}$$

increases linearly as length increases. As a result of this relationship, the longer you wish to move the pin up the chamber, the higher the hydraulic resistance is in the channel and therefore, the more pressure is needed to be produced by the pump. For these reasons, a full hydraulic solution does not seem a practical direction for manufacturing. Finally, pneummatic actuators have not shown precise position control which is needed in manufacturing.

2.4.4 Piezoelectric

Piezoelectric materials are materials that exhibit expansion or contraction when exposed to a voltage difference. There are two main benefits that make piezoelectrics a plausible solution at first glance; 1) they can achieve extremely fine positioning, 2) they can be miniaturized into very small pixels and placed into an Integrated Circuit Board. However, the maximum movement that can be achieved is 10% of the length of the material [33], which would mean a very long pin which requires a lot of voltage for a small amount of movement. The second major issue with a piezoelectric solution is that it is both expensive and fragile, which works well in compression, by poorly in tension [32].

2.4.5 Linear Motors

A linear motor is similar to an electric motor, but instead of producing torque through rotation, it is unraveled to produce a linear force along the direction of motion. As a

Figure 2.9: Three phase electrical conductors are placed in geometrical positions to create rotation by rotating the magnetic field. [22]

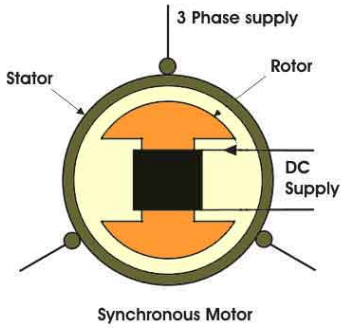

result, it follows the Lorentz Force relationship:

$$F = q[E + (v \times B)] \tag{2.3}$$

where q is the charge of the particle, E is the strength of the electric-field that the particle is exposed to, v is the velocity of the particle and B is the strength of the magnetic-field that particle is being exposed to. Given non-zero values, the particle in question will then experience a Lorentz Force, perpendicular to its direction on motion. It is obvious that a current is in fact charged particles (electrons specifically) in motion and the Lorentz Force equation is reduced to:

$$F = IL \times B \tag{2.4}$$

where I is the current in Amps and L is the travel distance of the current in the exposed magnetic field B. Using Lorentz Force, there are two types of motors that exists; Synchronous motor and Homopolar motor. The Synchronous motor works by controlling the movement of the magnetic field, B, to induce linear movement. Examples of Synchronous motors include coil guns and the maglev system. Though a practical solution, the inherent difficulty in miniaturizing coils for microfabrication make such a design unappealing, though plausible.

Alternatively, Homopolar motors work by varying the amout of current being applied in the magnetic field. One of the major applications for Homopolar motors is research being conducted by the U.S. Navy into Railguns [43]. The railgun works by charging an array of capacitor bays, and quickly discharging, exposing a projectile of interest to high

Figure 2.10: Physics of a Railgun. High current passes through the system and interacts with itself to create force. [30]

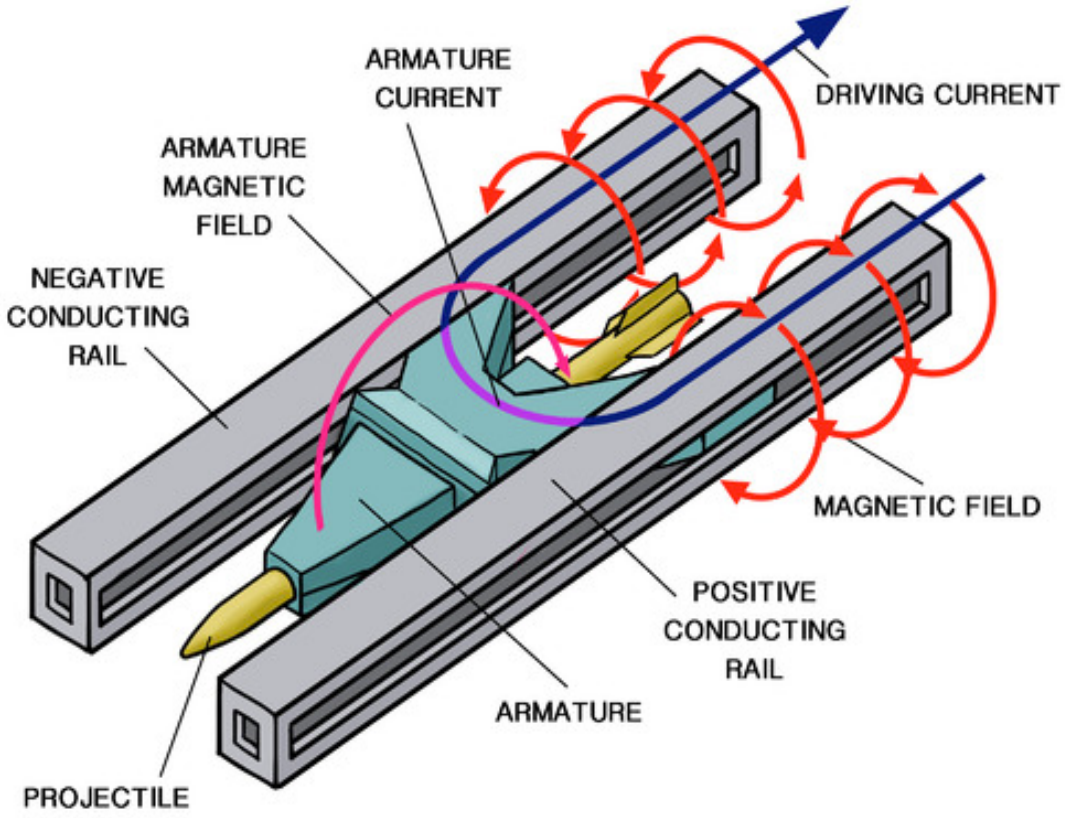

amounts of current. The current passing through the projectile interacts with the magnetic field produced by the current as it travels along the length of the chamber, creating a force that accelerates the projectile down the chamber, leaving the chamber at very high velocities [42].

2.5 Control System

2.5.1 Control

The purpose of the control system is to route current from a single power source to a pin, for microseconds to milliseconds at a time. This strategy is known as rasterization and the design is analogous to the addressing system used by Active-Matrix Organic Light Emitting Diodes (AMOLED) [18], in which to address a Pin, it's corresponding row and column transistors are turned on simultaneously to direct current into that Pin's cavity. For example, turning on T5 and T20 in the figure below will address the first pin in this system. Current will only travel into a pin when both transistors are in the ON position, otherwise the circuit will be open.

The main divergence our system has from typical AMOLED configurations is it's requirements of current in the order of amps rather than in milliamps. The advantages of a single a system that addresses a single pin at a time rather than multiple pins simultaneously are as follows:

1. Current is not divided; As the pins act as resistive loads in the system, addressing multiple pins simultaneously require higher amounts of power. 2. Easier to control; though addressing a single pin at a time requires faster refresh rates, this control strategy has been significantly developed for other uses (i.e. AMOLED), and is easier to position. In order to to determine where a pin will end up after current is being applied, we need to convert the acceleration of the pin from Lorentz Force into a position value, which is a second order differential calculation. This relationship can be simplified and ignored if a consistent, reproducible pulse is used. 3. It has been documented that a system can increase its current tolerance if it is pulsed rather than continuously applied (by a factor of 100) [17]. There is two leading ideas to explain this property: a) A pulsing current allows the system to cool down in-between pulsing cycles or b) a pulsing current turns off before the system can heat from the electron collisions.

The system also controls the direction of the current using an H-bridge; allowing the system to apply positive current to accelerate the pin upwards and negative current to accelerate the pin downwards (or decelerate it if necessary).

The H-Bridge uses a combination of MOSFET's to control the direction of current. When opposing MOSFET's are activated (diagonal to one-another), they result in current of one direction for V_cc, while the reverse configuration results in an opposite current being induced. Though H-bridges can be bought of the shelf, they are mostly used for rotational

Figure 2.11: Example control circuit

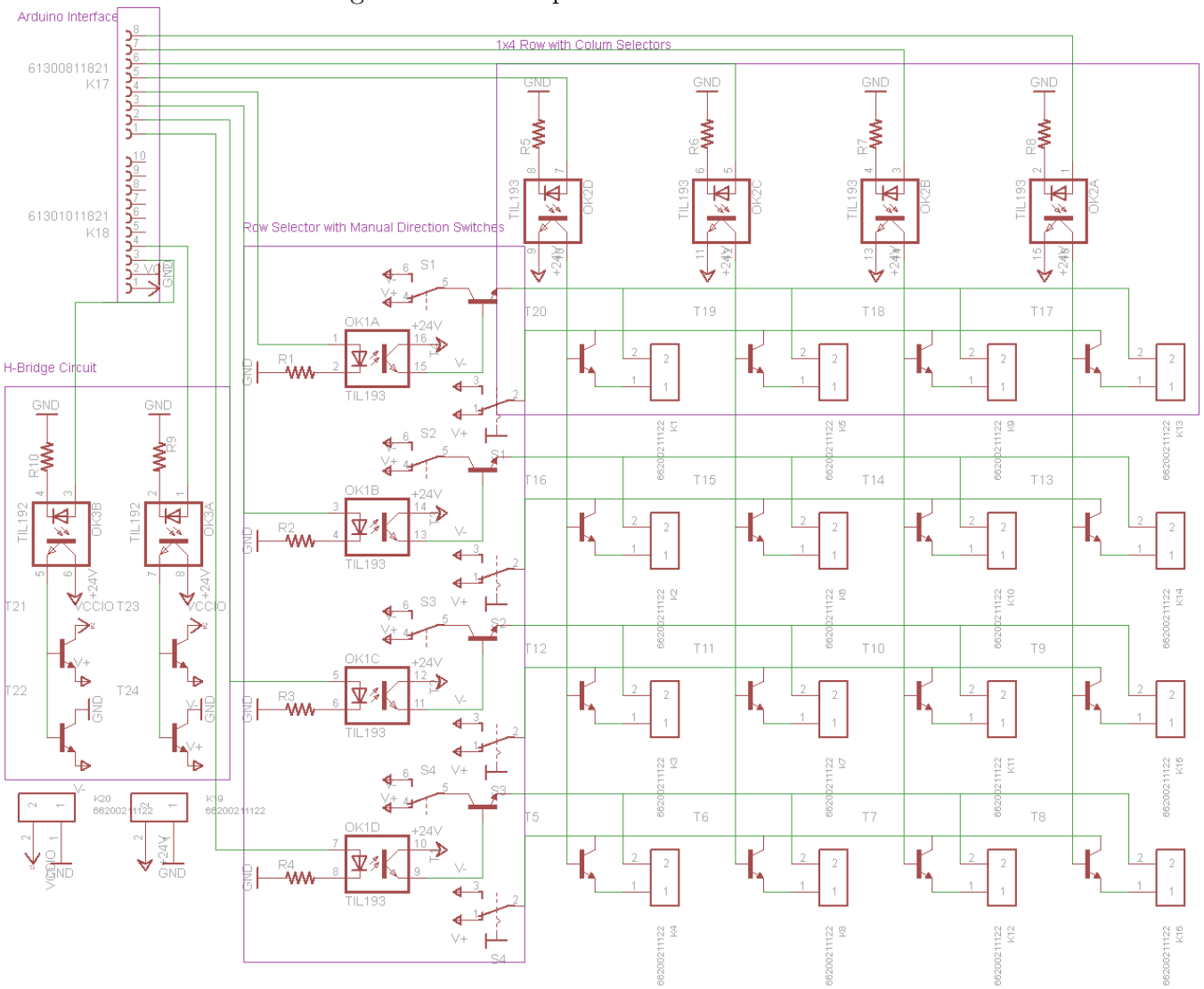

motors, and therefore tend to have far more complex circuitry required to fulfill features needed for electric, rotational motors.

Optoisolators is a circuit component that uses an LED (or any other optical transmitter) to create an electrical signal between to separate electrical system, while keeping them electrically isolated from each other. In our use case, the optoisolators are being used for Transistor-transistor Logic (TTL) to step up from 5V to 24V which is needed for the addressing MOSFET's. This allows the system which controls the digital logic (such as a microcontroller) to convert the 5V signal to a high 24V signal. The higher voltage needed by the addressing MOSFET's is due to the need of a higher gate voltage in the MOSFET's to offset the higher channel voltage in the system.

2.6 Locking Mechanism

2.6.1 Fluid Locking System

The hydraulic support system compromises of a plurality of cavities that are below the rail motor section of the system, extending the system further. The end of each pin, exposed to the hydraulic layer of the system is fitted with a hydraulic plug which acts as a slidable sealant, ensuring the liquid doesn't leak out of the system. The opposite end of the cavity terminates in an inverted frusto-conical valve aperture

The valve block is coupled to a support block that is remote from the guide structure. The valve block is coupled with an actuator (a large, commercially available actuator), that acts as a universal sealant, closing all the apertures simultaneously, once the pins are in their desired position. This is achieved because the valve block has a plurality of spaced apart conical valving members that are arranged to match the frusto-conical valve apertures in the hydraulic layer of the system. The cone valves are in constant fluid communication with a constant pressure reservoir via an adjustable volume and fluid transfer conduits, which communicate adjustable volume and constant pressure reservoirs. By introducing fluid into the cavities and sealing the fluid within the cavities, support is provided to the pins. Inversely, by withdrawing fluid from the cavities, the pins are released from their assigned position.

Figure 2.12: Diagram of how fluid locking works [36]

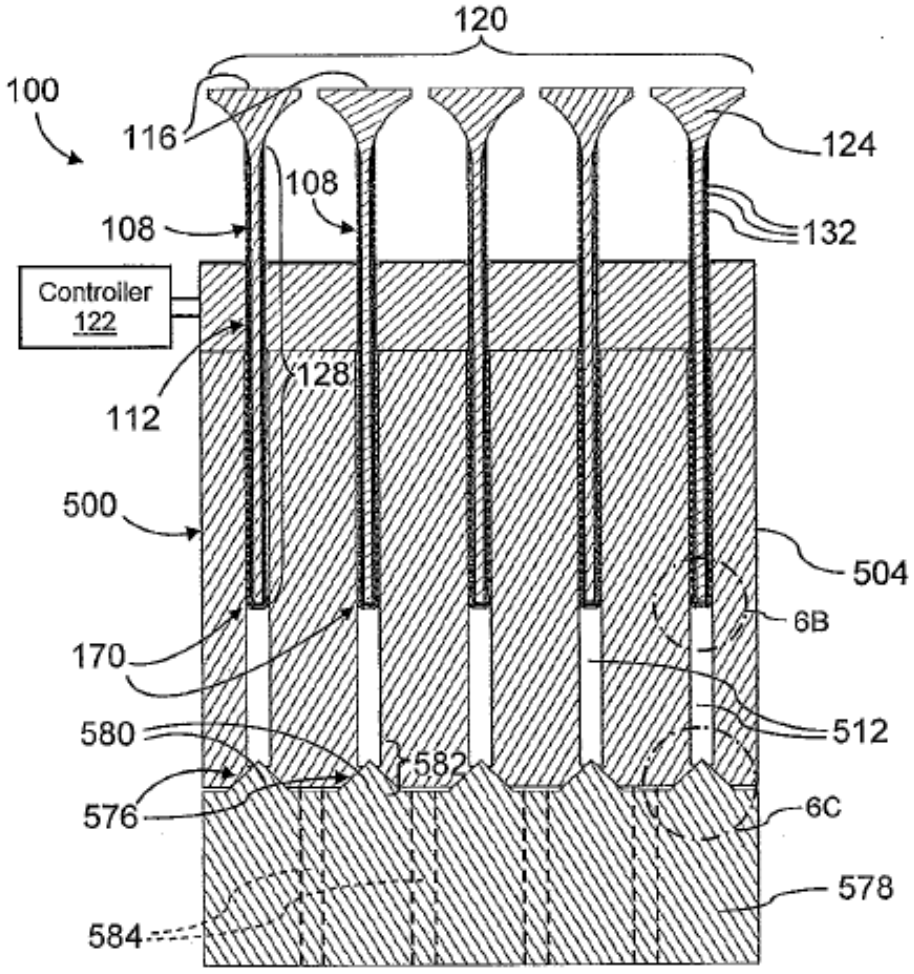

2.6.2 Gel-based Clamping System

A secondary locking mechanism can be used to hold the pins in position when the cavity beneath the pin is being filled with fluid. The strategy is analogous to a vice grip and works by using an elastomeric membrane with a high poisson ratio; a material that expands significantly in the two directions perpendicular to the direction of compression. Once the pins are in position, the elastomeric material, which is sandwiched between the hydraulic block and the rail motor block, is compressed by applying opposing forces on. This in turn forces the elastomer to expand into the cavity (since it is the direction of least resistance) and squeeze around the pin; providing a frictional force (analogous to a vice grip) to prevent the pin from moving. Though this mechanism can be used to hold the pin in position, it does not provide enough force to overcome the force of manufacturing. It also acts as a layer to prevent leakage.

2.7 Model

The following section's purpose is to define the model that will be used by Microhydraulics SMT solver to generate solutions for various environments the programmable die will be used in. The largest difficulty with generating solutions for programmable dies is that the solution is not for a single application but rather a range of applications the system will be used for. The microfluidics models have been ignored in this section as the models have already been thoroughly developed in the single-phase and multi-phase sections of this thesis.

2.7.1 Dimension Restrictions

In many of the targeted applications in manufacturing, the reconfigurable tool will have to exist within a predefined volume. Therefore, generated designs of the system must stay within restricted dimensions ($h \times w \times l$). This is done by using a cartesian coordinate system, with defined boundary conditions to describe the volume the system can occupy. Typically, the predefined volume can be defined by setting a maximum h, w, and l.

2.7.2 Resolution and Step Size

The pin resolution and step size are determined by the application. In the cases a small step size is needed, a heavier pin is used as the step size of of the pin is determined by both

Figure 2.13: As two plates press against each other, the gel pushes againsts the pin [36]

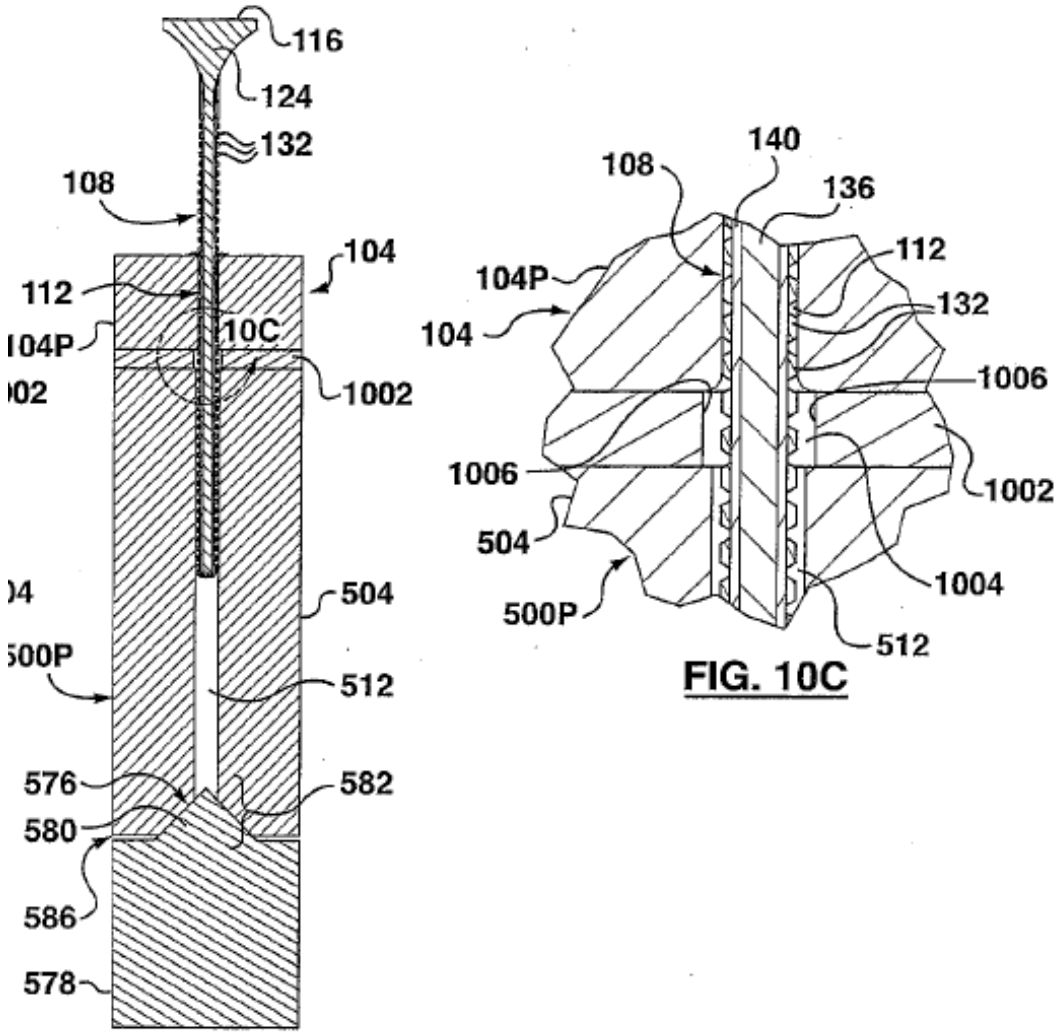

the minimum force required to overcome static friction divided by the mass of the pin as follows:

$$Step = \frac{F_{min}}{M} \tag{2.5}$$

The resolution is essentially the area of the pin head, and determines the cost of each pin. As the pin gets smaller, different fabrication methods need to be used and the cost of each pin increases.

2.7.3 Interpolating Layer

When selecting an interpolating layer or an elastomeric sheet, many factors need to be considered. The purpose of the interpolating layer is to serve as a smoothening mechanism between linear actuators. For extrusion, where a fluid passes through a die, the fluid eventually becomes solid after passing through through a UV or thermal curing process. Without the interpolating layer, leakage may occur when dealing with wet processes as well increased roughness in the finished material (staircase effect that is dependent on pin resolution).

In order to determine the ideal material to be used as the interpolating layer, a strain analysis must be completed using FEM numerical methods [50]. Along with ideal material selection, the required thickness of the material is also relevant. For complete smoothening of the surface, the minimum material thickness is equal to the area of the head of the linear actuator. A model used often for hyper-elastic material ideal for use as the interpolating layer is the Mooney-Rivlin Solid model [64].

$$W = C_1(I_1 - 3) + C_2(I_2 - 3) \tag{2.6}$$

W is the deformation energy in the system, C_1 and C_2 are empirically determined material constants and I_1 and I_2 are the first and second invariant tensors of the left Cauchy-Green deformation tensor [60] defined as:

$$B_{ij} = \frac{\partial x_i}{\partial X_K}\frac{\partial x_j}{\partial X_K} \tag{2.7}$$

The goal of the system would be to minimize the potential energy in the system which takes the form of deformation energy W.

2.7.4 Buckling

Since each pin behaves as a column supporting the material that is being shaped, buckling analysis needs to be completed in order to ensure that the pins do not buckle under pressure. The maximum critical force that can be applied to a pin is called Euler's critical load and is calculated as follows [63]:

$$F = \frac{\pi^2 EI}{(KL)^2} \tag{2.8}$$

Where F is the critical force that can be applied on each pin, E is the modulus of elasticity, I the area moment of inertia, L is the unsupported column length and K is the column effective length factor.

2.7.5 Lorrentz Force

Lorrentz Force equation was defined earlier as follows [62]

$$F = ILB \tag{2.9}$$

Where F is the force, I is the current in amps and L is the length of current exposed to a magnetic field B. The objective in most applications will be to increase the Lorrentz Force to as high as possible. This is achieved by maximizing the amount of current is exposed to a perpendicular magnetic field. As a result of this relationship, a longer pin will generate more force as it increase the value of L. Though this would suggest you should make a long pin, a long pin has dimension restrictions as well as buckling factors that need to be considered.

2.7.6 Joule Heating

Another way to increase the Lorrentz Force in the system is by increasing the amount of current running through the pins. Increased current, however, has the undesired effect of Joule Heating. Joule Heating is defined as follows [61]:

$$P(t) = I(t)^2 R \tag{2.10}$$

Where P is the instantaneous power being converted to heat in time t, I is the current and R is resistivity which in this case is the resistivity of the wire. Joule heating deteriorates the pin as it causes burn marks through arcing or electromigration [57]. Increase in heat also effects the permanent magnets as around most magnets begin to demagnetize at temperatures above 80 degrees Celsius [40].

2.8 Physical Prototypes

2.8.1 Wired Prototype

Our initial proof-of-concept was developed to demonstrate Lorentz force for ourselves for the sake of pin actuation. We used a CAD software to design a 3D printed enclosing to hold permanent magnets, and pushed a thin wire with 5 amps of current through it. This initial prototype was successful in demonstrating Lorentz Force as well as illuminated us to the fact that a design that used electric wires would require a wire with high elasticity.

2.8.2 Pin Array Prototype v.1.0

Our first prototype was a 10 x 10 array of pins with an assortment of magnetics. This prototype turned out to be a complete failure. With learnt with this prototype that we could not perfectly align all the magnets in one direction since magnets prefer to be oriented north to south, not north to north. Also, the additional force more magnets exerted on the guide structure destroyed the enclosure.

2.8.3 Pin Array Prototype v.1.1

In our third iteration of the pin design, we created a 3x3 pin array with a single column of magnets. This avoided the need for aligning the magnets and provided a good demonstrate of the concept. We also discovered with this design that the magnetic field near the edges of the magnet suffered from edge effects and did not align in the targeted orientation. This resulted in the force acting on the pins near the corner to be parallel with the magnets, perpendicular to our direction of interest.

2.8.4 Rolling Contact Pins

Our fourth prototype moved away from wired pins and moved towards rolling pins. We used a brass to conduct electricity between to electrical contacts. This proved to have the following challenges:

1. *Ensure electrical contact*; We could not ensure vertical electrical contact, and therefore were restricted to only a horizontal solution.

2. *Sparking/Burning:* The high current passing through the electrical contacts into the pins proved to be difficult. High voltage and current created a huge power dissipation in the system which resulted in burning and if the surface was not relatively flat, bumps would cause sparking which in turn caused melting. We found jewelers cloth to be the best tool to smoothen out the brass rod and the electrical contacts.

3. *Lubricants:* We tested out conductive lubricants, but these turned out to be more of a hindrance than an aid. This is because at the micrometer level that we are dealing with, the additional viscosity of the fluid as well as the additional roughness the lubricant decreased the efficiency of the system.

4. *Materials:* We attempted to use steel instead of brass, assuming that the magnetic field from the permanent magnet would ensure sliding contact. However, since the field is not uniform across the surface of a permanent magnet, the steel rod was attracted to the center of the magnet, and could not be moved.

2.8.5 PID

A Proportional-integral-derivative controller (PID controller) is a common methodology used in control systems. In has three main terms, a proportional term, an integral term and a derivative tern. These terms are used to compensate for the error that the system would differ from the ideal scenario. The proportional term is used to compensate for the error at the current time step, the integral term compensates for the overall error in the system and the derivative term compensates for the change of error between measurements. The overall equation is as follows:

$$u(t) = K_p e(t) + K_i \int_0^t e(\tau)d\tau + K_d \frac{d}{dt} e(t) \tag{2.11}$$

where $u(t)$ is the controller output, K_p is the proportional gain tuning parameter, K_i is the integral gain tuning parameter, K_d is the derivative gain turning parameter, e is the error, t is the time, and τ is the variable of integration.

A comparison of the PID methodology vs a table lookup strategy was completed in order to determine the trade-offs between the two strategies. PID proved to be better solution because it could compensate for production quality issues. The feedback mechanism used was a variable resistor, which has the relationship:

$$R = \frac{\rho L}{A} \tag{2.12}$$

where R is the resistance, L is the length of the resistor, A the area of the resistor and ρ is the surface resistivity. Initially, three variable resistors were tested, pencil lead, carbon tape and vhs tape. The following graphs show the results of these tests. The carbon tape showed the most consistant result.

The table lookup strategy worked well after a calibration since the carbon tape showed a consistent linear relationship of approximately 97Ω/mm. An initial calibration run was down by slowly moving the pin while taking out voltage readings at each point. A combination of calipers and video recordings was used to measure the distance the pin had moved. In comparison, the PID worked best when the integral and derivative terms were set to zero, seen in the following graphs (figure 2.15:

Figure 2.14: Picture of the first wire based prototype

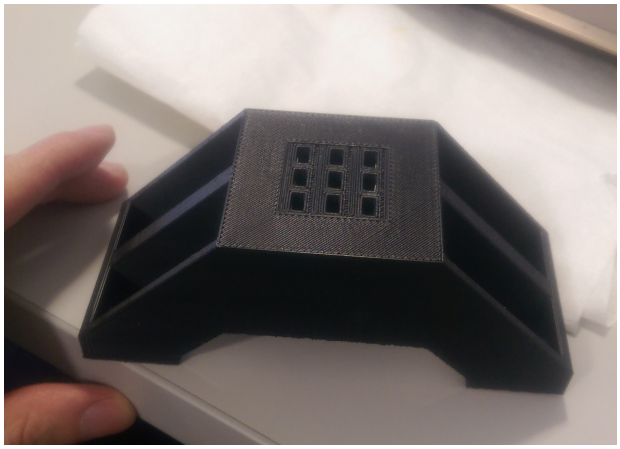

Figure 2.15: Most recent state of Prototype

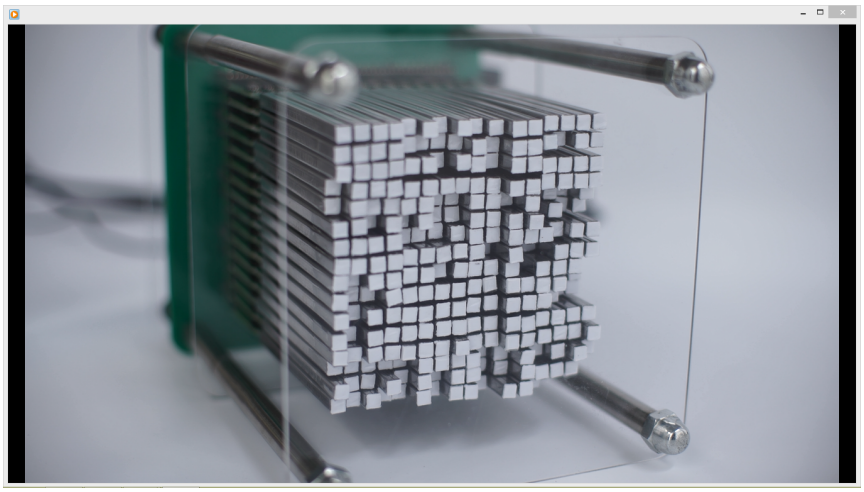

2.9 Previous Works

2.9.1 Railguns [Rail Motors]

Railguns are known to operate at thousands of volts, generating large amounts of current sustained for a few milliseconds in order to accelerate a small projectile. Alternatively, with the advent of solid-state switches and ultra-capacitors, there has been emergence of low voltage railguns, otherwise known as rail motors, that can operate for longer periods of time (on the scale of seconds), accelerating much larger loads [55].

One of the difficulties with rail motors is ensuring that the electrical contacts between the projectile and the current source. The reason this poses less of an issue for railguns is simply because the high voltage used in rail guns allow current arcing to overcome the gap between the projectile and the electrical contacts. One strategy to overcome this issue is to provide a force that pushes to projectile into the electrical contact. This force can either be achieved through creating tight spacing between the electrical contact and the projectile to allow for the natural elasticity in a material to ensure electrical contact. Another strategy is to design the projectile in a way that allows the Lorentz force produced to be slightly directed into ensuring electrical contact.

An example of potential designs for projectiles are seen in [55]. Of these designs, [55] reports that the X design seemed to perform the best.

Using a rail motor design, [68] reported being able to accelerate a 2 mm polycarbonate cube to 5.7 km/s in 20 seconds. The main strategy that helped [68] achieve hypervelocity is through the use of an external pulsed magnetic field, which in magnetrons [17], has shown to lead to substantially higher magnetic fields. This is because the current being sent through the system is substantially higher since the current is turned off before permanent material damage is done to the system.

2.9.2 Reconfigurable Pin-Type Tooling

Rapid and reconfigurable tooling slides; Cyril Bath's use an interpolating layer to compensate for the space between pins. The effectiveness thickness is defined by the thickness of the interpolating layer after elastic deformation has occurred.

2.9.3 Pin Design

According to [59], there are four things a good pin design requires:

1. Pins should have uniform cross-section shape, size and length to minimize cost and lead time.
2. Pins should be strong enough to withstand buckling.
3. The pins should form a rigid surface when stationary and locked.
4. The cross-sectional area of the pin should be as small as possible for achieving the highest amount of shape fidelity.

Pin tips should not be sharp to prevent penetration of the interpolating layer, making spherical pin heads an ideal solution. Two standard solutions exist for the distribution of the pins. The pins can be either distributed as a matrix of uniformly spaced pins or as a matrix of closed-packed pins.

Figure 2.16: Methods a matrix of pins can be distributed [59]

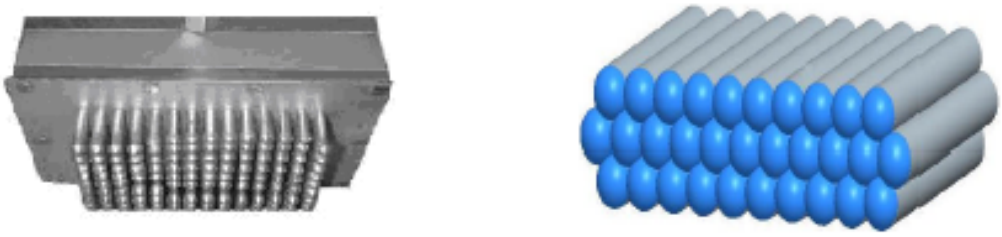

Though closed-packed distribution has the advantage of being able to handle substantially more force, individual actuation of each pin becomes substantially more difficult.

Chapter 3

Single-Phase Microfluidic Circuits

Microfluidic chips, lab-on-a-chip devices that have channels transporting liquids instead of wires carrying electrons, have attracted considerable attention recently from the biomedical industry because of their application in testing assay and large-scale chemical reaction automation. These chips promise dramatic reduction in the cost of large-scale reactions and bio-chemical sensors. As in computer chip design, there is an acute need for automation tools that can assist with design, testing and verification of microfluidic chips. The current state of practice is that microfluidics chips are designed manually using a guess-and-check approach. We propose a design methodology for microfluidic chips based on SMT solvers, with the goal of producing designs that are correct by construction. The design of these chips is expressed using the language of partial differential equations (PDEs) and non-linear multi-variate polynomials over the reals. We convert such designs into SMT2 format through appropriate approximations, and use Z3 and dReal to solve for the unknown design parameters.

3.0.4 Pressure and Flow Constraints

The microfluidic designer is concerned with the pressure (P) at nodes and the rate of flow (Q) along channels. These are related to each other by the hydrodynamic resistance of the channel (R) like so:

$$P_i = P_j + (-1)^{\phi} Q_{ij} R_{ij} \tag{3.1}$$

where i and j name two adjacent nodes and the $(-1)^{\phi}$ factor simply indicates the direction of flow in the channel.

The chip designer will specify some of the pressures (P) and flow rates (Q) and leave the rest to be computed by our system. The solver will also compute the channel lengths, which are a factor in the hydrodynamic resistance (R). The designer may restrict the tolerable limits for any of the values to be computed.

The hydrodynamic resistance (R) of a channel is a function of the shape and size of the channel, as well as the material used to build the channel. For cylindrical channels the size is characterized by the radius (r) and the length (L). For rectangular channels the size is characterized by the width (w), height (h), and length (L). The important property of the fluid is its coefficient of frictional resistance (μ). Equation (3.2) relates these factors:

$$R = \begin{cases} \frac{8\mu L}{r^4} & \text{cylindrical channel} \\ \frac{12\mu L}{wh^3(1-0.640\frac{h}{w})} & \text{rectangular channel} \end{cases} \tag{3.2}$$

Finally, the instruments being attached to the chip and the chemical reactions occurring in the chip might place constraints on the minimum acceptable volume for certain channels.

3.0.5 Placement Constraints

The nodes must be positioned on the chip in such a way that respects the desired topology, the required channel lengths, the physical size of the chip, the permissible angles between channels, specific required locations of certain nodes, and specific required intersection points for certain channels. The specific placement constraints arise due to interaction of the chip with external devices.

The Cartesian coordinates of two connected nodes i, j are constrained by the length L_{ij} of the channel between them according to the Pythagorean theorem. Suppose the channel between nodes i and j is required to pass through a position p on the chip, identified by the coordinates $\langle x_p, y_p \rangle$. We simply constrain the triangle defined by the three points i, p, and j, to have no area:

$$x_i(y_p - y_j) + x_p(y_j - y_i) + x_j(y_i - y_p) = 0 \tag{3.3}$$

Microfluidic circuits often require cyclic paths. We lay these out as polygons composed of adjacent triangles that meet at center point c. For each pair of connected points i and j

around center point c, the law of cosines and the definition of cosine in terms of dot-product tells us:

$$\begin{aligned} |\overrightarrow{ij}|^2 &= |\overrightarrow{ci}|^2 + |\overrightarrow{cj}|^2 - 2|\overrightarrow{ci}||\overrightarrow{cj}| \cos\theta_{ij}^c \\ &= |\overrightarrow{ci}|^2 + |\overrightarrow{cj}|^2 - 2|\overrightarrow{ci}||\overrightarrow{cj}|(\tfrac{\overrightarrow{ci}\cdot\overrightarrow{cj}}{|\overrightarrow{ci}||\overrightarrow{cj}|}) \\ &= |\overrightarrow{ci}|^2 + |\overrightarrow{cj}|^2 - 2(\overrightarrow{ci}\cdot\overrightarrow{cj}) \end{aligned} \tag{3.4}$$

For the generated constraints, the dot-product and the magnitudes of the vectors are expanded in terms of the Cartesian coordinates of the points. The manufacturing process imposes a minimum possible channel length, whereas the chip size imposes a maximum possible channel length. A minimum angle between channels connecting to a common node is enforced to prevent fluid in the channels from inadvertently mixing.

3.1 Sensing

3.1.1 Beer-Lambert Law

Microfluidic scientists find the absorption of electromagnetic radiation for certain molecules important, as it can be used to determine the presence of a molecule in a solution. The intensity of the absorbed electromagnetic radiation is given by:

$$I = \frac{energy}{area \times time} = \frac{J}{m^2 s} \tag{3.5}$$

Whenever the frequency of the electromagnetic radiation matches the difference between the energy levels of the two outer most electron transition states of the molecule of interest, the molecule will absorb the radiation. This relationship is given by:

$$hf = E_j - E_i \tag{3.6}$$

where E_i and E_j are the energy levels of interest, f is the frequency of electromagnetic radiation and h is Planck's constant. Whenever the molecule absorbs the radiation, the transmittance level T of radiation falls below the background level of radiation I_0.

$$T = \frac{I}{I_0} \tag{3.7}$$

This means that the molecule has absorbed the radiation, the negative log of transmission, and this can be related to the concentration of the molecule c_m in the system through Beer-Lambert's Law.

$$A = -log(T) = log\frac{I}{I_0} \tag{3.8}$$

$$A = log\frac{I_0}{I(l)} = \varepsilon l c_m \tag{3.9}$$

Here, l is the length of the medium parallel to the radiation source, and ε is the absorptivity proportionality constant for the molecule.

3.1.2 Signal-to-Noise Ratio

In order to differentiate the detection signal vs. background noise, we need to determine the quality of the signal by analyzing the signal to noise ratio. The signal-to-noise ratio, SNR, is determined by the following equation:

$$SNR = \frac{S_{max}}{3\sigma} \tag{3.10}$$

Here, S_{max} is the maximum strength of the signal in question and sigma is the standard distribution of the signal, assuming a Normal Gaussian distribution. The limit of detection LOD, is equal to 3σ, and is the lowest quanitity of a signal that can be distinguished from the absence of a signal.

3.2 Electroosmotic Flow (EOF)

Applying an electric field across capillaries or microchannels results in bulk fluid motion. The fluid flow velocity has a linear relationship that is dependent on both the material of the chip and the fluid flowing through the chip's channels. This flow is refereed to as electro-osmosis flow and is motivated by the Electric Double Layer (EDL) effect. Though this flow is simpler to control than minaturized mechanical pressurized pumps, it's velocity distribution differs from pressure-driven flow and is sensitive to the chemical properties of the interface (between chip and fluid) and to Joule heating.

3.2.1 Joule Heating

Also known as ohmic heating or resistive heating is when a conductor of electric current releases heat. The amount of heat released is proportional to the square of the current. This is of concern in microfluidic devices since excessive heat can cause damage to the chip, or unpredictable reactions/flow rates. Current through a conductor generates heat S_{JH} through the relationship:

$$S_{JH} = \sigma E^2 \tag{3.11}$$

Where S_{JH} is the watts per unit volume (W/m^3) and σ is the conductivity of the medium. In the case of cylindrical channel, heating across the channel due to joule heating is:

$$T(r) = \frac{E^2 {r_0}^2}{4\rho\kappa}(1 - \frac{r^2}{{r_0}^2}) + T_0 \tag{3.12}$$

where r_0 is the radius, T_0 is the temperature (in celcius) of heat-sink on the chip, ρ is the resistivity, and κ is the inverse of the thermal coefficient of expansion. In the case of a polymeric cylinder, the equation:

$$T(r) = \frac{{r_i}^2 \sigma E^2}{2\kappa} lnr + K_2 \tag{3.13}$$

where K_2 can be determined by setting the temperature of the outer radius r_0 to room temperature. r_i is the radius of the microchannel. In spherical coordinates, with a heat sink at the outer radius (i.e. room temperature):

$$T(r) = \frac{-S_{JH} r^2}{6\kappa} + K_1 \tag{3.14}$$

where K_1 can be determined by solving for what the temperature is and the outer radius r_0 (i.e. room temperature)

3.2.2 Outer Solution Fluid-flow

Though the full description of the fluid flow in electroosmosis is dependent on solving the Navier-Stokes equation, substituting the force component with Coulombic Force interactions and solving both the Poisson equation and the Boltzmmann distribution of ions

simultaneously, simplifications allow us to describe the "Outer Solution Fluid-flow"; which resides in the flow of the solution far from the wall.

The Electric Double Layer (EDL) is the thin layer of ions that is generated near the wall of the channel when the channel wall is exposed to an aqueous solution. This is the driving force behind the "Inner Fluid-flow", and the cause of the resulting velocity gradience and vorticies seen near the channel edges.

The 1D inner solution for electroosmosis results in:

$$u_{inner} = \frac{\epsilon E_{ext,wall}}{\eta}(\varphi - \varphi_0) \tag{3.15}$$

where u_{inner} is the flow rate near the walls of the channel affected by EDL, ϵ is the electrical permitivity of the solution, η is the dynamic viscosity of the solution and φ and φ_0 are the electric potential difference from bulk and total potential drop across the double layer respectively.

The thin EDL approximation is often used in micro-channels since the effects of the EDL can be approximated out of the Outer Solution-flow. This is known as ideal Electroosmosis Flow (EOF). There are four conditions that need to be met in order to assume ideal EOF. (i) the ζ potential must be a constant near the channel walls, (ii) the electric field must be uniform (iii) the system must be is steady-state and (iv) the Debye length, λ_D, must be smaller than the channel of the radius or half the width of the channel. This simplification leads to the Helmholtz-Smoluchowski equation, which sets $\varphi_0 = 0$, resulting in:

$$u = -\frac{\epsilon\varphi_0}{\eta}E_{ext,wall} \tag{3.16}$$

Electroosmotic mobility, μ_{EOF} is used to describe the linear relationship between flow rate and the applied electric field, defined by:

$$\mu_{EOF} = -\frac{\epsilon\varphi_0}{\eta} \tag{3.17}$$

In literature, it is common to report the zeta potential, ζ , which can be deducted from μ_{EOF}:

$$\zeta = -\frac{\mu_{EOF}\eta_{bulk}}{\epsilon_{bulk}} \tag{3.18}$$

It should also be noted that electroosmosis flow also stimulates pressure in the channel.

3.2.3 Diffusion

Diffusion is a time-dependent phenomena. Is the motion of solute in the solvent from regions of high to low concentrations. Result of thermally induced thermal motion such as Brownian motion

Fick's second law dictates how concentration will change as a Gaussian over time, following the relationship:

$$C(x,t) = \frac{C_0}{2\sqrt{D\pi t}} e^{\frac{-x^2}{4Dt}} \tag{3.19}$$

with a standard deviation σ of:

$$\sigma = \sqrt{2Dt} \tag{3.20}$$

where C_0 is the initial concentration of the system, and D is the diffusion constant that varies over time, and x is the location across the channel. x can be replaced by $x - vt$ if the solute is being moved by an electrophoretic process.

3.2.4 Peclet Number

The Peclet number, $Pé$, is a number used to determine how flow due to diffusion compares to flow due to convection. It is simply defined as:

$$Pé = \frac{diffusiontime}{convectiontime} = \frac{vL}{D} \tag{3.21}$$

Diffusion is dominant when the $Pé \gg 1$ and negligible when $Pé \ll 1$. The Peclet Number can be used to determine when diffusion needs to be considered by the system and when diffusion is negligible and can be ignored from design analysis.

3.2.5 Electrophoretic Movement

Electrophoresis drives charged molecules through a channel via Coulomb forces, which is countered by Stokes drag. This motion is proportional to an electric field and in steady state, the forces in the system equalize, resulting in the relationship:

$$v = \mu_{EP} E \tag{3.22}$$

where v is the velocity of the system, E is the electric field applied across the channel and μ_{EP} is the molecule's mobility due to electrophoresis. Particles, as opposed to molecules, cannot use this model as they have a large enough charge to create a continuous EDL. The μ_{EP} comes from the constant terms that arise from combining the Coulomb Force equation and the Stokes drag equation and is described as follows:

$$\mu_{EP} = \frac{q}{6\pi\eta r} \tag{3.23}$$

In the general case, the mobility of the molecule is the sum of the mobility due to electrophoresis and the mobility due to electroosmosis.

$$\mu = \mu_{EOF} + \mu_{Ep} \tag{3.24}$$

3.3 Microchip Electrophoresis

A single-phase implementation of an electrophoresis crossing was explored. A current limitation that Chris Backhouse's Microfluidic research group at the University of Waterloo faces is the inability to quickly explore the design space of the electrophoretic croses due to the numerous variables and the complicated mathematical relationships they have with one another. As a result, often times they simply guess a design that may seemingly work, build it, and test it to see if the results are favourable to what is needed.

Electrophoresis works by prorogations charged molecules forward through the use of an electric field. Depending on the properties of the molecule(s), the resulting rate of propagation will vary. The rate of propagation or velocity is dependent on many factors, most importantly on the viscosity of the medium, the charge-to-mass ratio of the molecule and the strength of the electric field the moelcule(s) are being exposed too. Electrophoresis is broken down into three sequence of events. The first step is the loading phase, and consists of distributing the molecule(s) of interest across the first channel. Often times the sample has already gone through a binding process to 'tag' molecules of interest. The second stage is called the injection phase, and entails injecting a portion of the sample into the channel perpendicular to the loading channel through the application of an electric field from the cathode reservoir to the anode reservoir. This is completed once a sufficient amount of the

Figure 3.1: An example electrophoretic cross. Sample is distributed across injection channel and then injected into the seperation channel. [14]

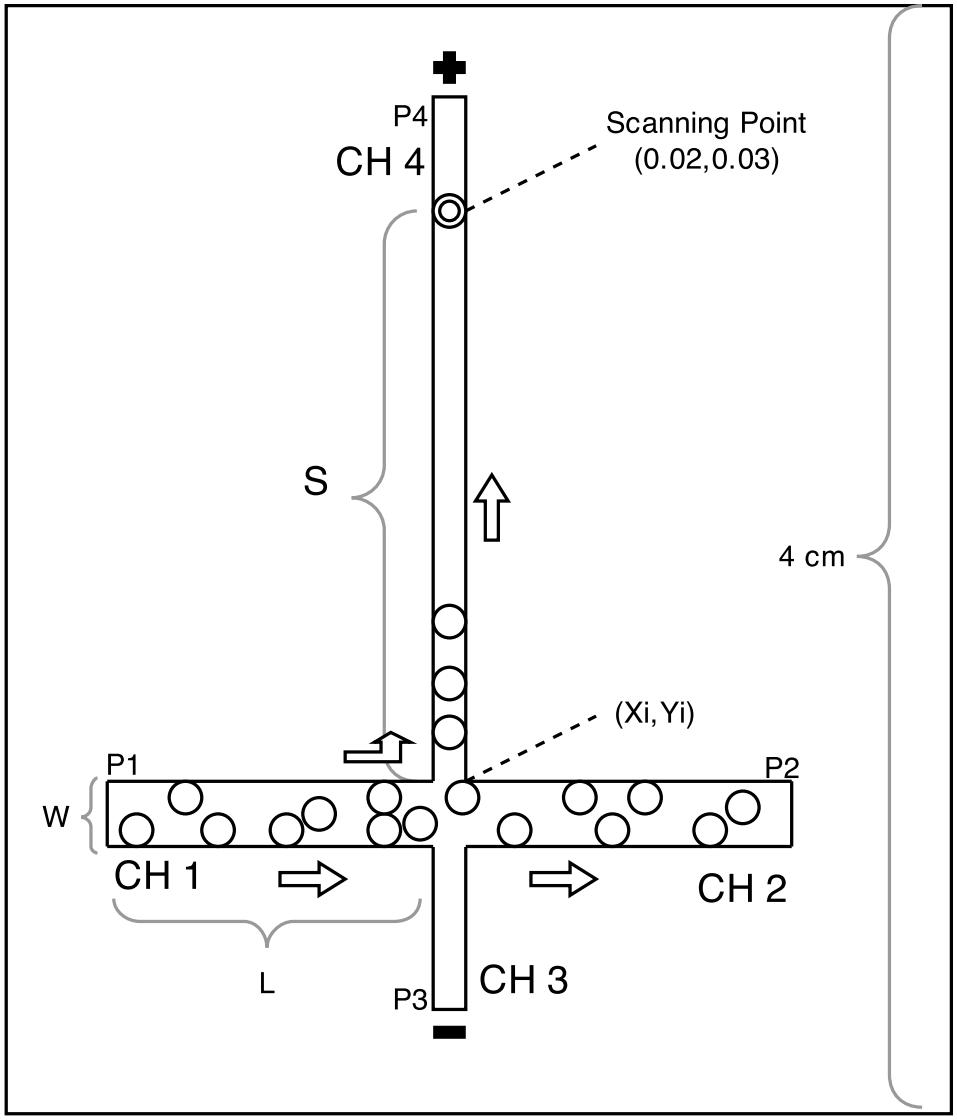

material being investigated has been transported across the intersection of the channels. The injected material (analytes) is called the sample plug, and in the separation phase, a potential difference between the anode and cathode reservoirs is maintained to stimulate the separation of analytes within the separation channel. A detector is positioned between the anode and cathode reservoirs (usually in closer proximity to the anode reservoir) in order to measure the analytes concentration at that location over time. The detection method can be a fluorescent one, and is achieved through the stimulation of the fluorescence in the molecule used for tagging the analyte of interest. The resulting plot is called an electrpherogramm and it is used to plot the concentration of analytes at the location of interest over time.

The following sections describe the mathematical description(s) used to describe an electrophoretic cross.

3.3.1 Analyte Movement in an Electric Field

A molecule in an electric field moves to the relationship: ;

$$\overrightarrow{v} = \mu \overrightarrow{E} \tag{3.25}$$

where $\overrightarrow{v}$ is the velocity of the molecule, μ is the (apparent) mobility of the molecule and $\overrightarrow{E}$ is the applied electric field [reference 4 - Stephen]. This relationship stimulates two types of movement. If the molecule is carries a net charge, the molecule being exposed to an electric field will motivate the molecule to move from an area of high electric potential to an area of low electric potential given that the molecule is negatively charged (the opposite relationship exists in the case of a positively charge molecule) such as the case of DNA. If the bulk fluid is charged, the same relationship can encourage flow of the bulk fluid, which in turn would cause the analyte to flow as well. The former is known as electrophoretic flow while the latter is known as electroosmotic flow. For the purposes of this model, we focus on electrophoretic flow.

The mobility of a molecule is then dependent on the summation of both the electrophoretic and electroosmotic mobility components as follows:

$$\mu = \mu_{EP} + \mu_{EOF} \tag{3.26}$$

where EP and EOF denote the electrophoretic and electroosmotic components respectively. The mobility of a molecule in a medium is quite dynamic and dependent on multiple

variables including the molecular charge, weight, shape and size. It is also highly dependent on the bulk fluid properties such as its pH, viscosity and composition. In general, a molecule that can be approximated as a sphere can follow the following relationship:

$$\mu_{EP} = \frac{q}{g\pi\eta r} \tag{3.27}$$

while electroosmotic mobility is usually approximated as:

$$\mu_{EOF} \approx 1.0 \times 10^{-8} m^2 s^- 1 V^- 1 \tag{3.28}$$

3.3.2 Movement of Sample Plug

As established earlier, the Sample Plug is the component of the sample that is injected from the electrophoretic cross during the injection phase for analysis. It's response to an applied electric field helps determine its properties. This system can be described as a two-variable function known as the concentration profile, which describes the concentration of the analyte at position x between the cathode and anode at time t. In an ideal case where there is an absence of all other physical effects except the properties that drive electrophoretic flow, the concentration profile would simply mimic that of the cross at time zero, since the moving sample would approximately have a uniform velocity across the system. Given these assumptions along with the idea that the sample is initially accelerated instantaneously, the initial concentration profile resembles:

$$C(x,t) = C(x - vt, 0) \tag{3.29}$$

where v is the velocity of the sample due to electrophoretic (and electroosmotic flow). However, in reality the sample diffuses over time as it moves down the channel. [5] shows that this can be modeled by:

$$\sigma(t) = \sigma_0 + \sqrt{2Dt} \tag{3.30}$$

where D is the diffusion coefficient of the interested analyte and:

$$\sigma_0 = \frac{r_{channel}}{2\sqrt{2\ln 2}} \tag{3.31}$$

Figure 3.2: The graph on the left is when $D = 0.1$ at $x = 40$ and all other parameters set to 1. The graph on the right is when $D = 1$ and $x = 40$.[14]

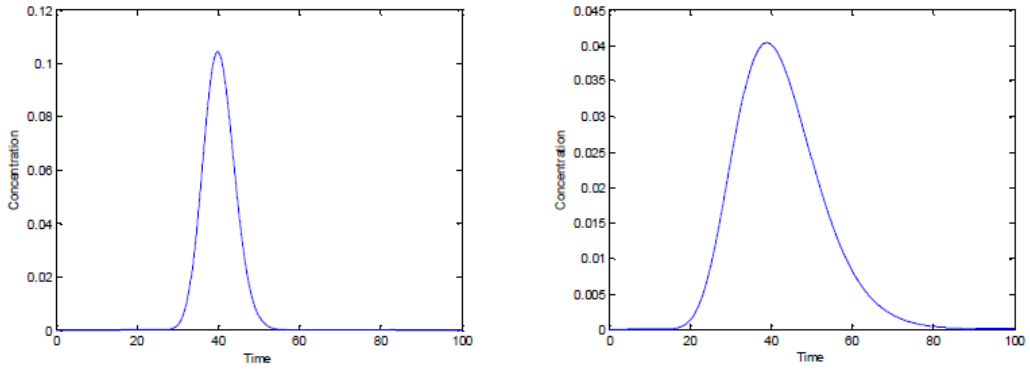

The concentration within the channel is then expressed as:

$$C(x,t) = \frac{C_0}{\sqrt{2\pi\sigma(t)}} \exp \frac{-(x-vt)^2}{2(\sigma(t))^2} \tag{3.32}$$

where C_0 is the initial concentration of the sample material originally injected into the separation channel. In the case where:

$$t \ll \frac{{\sigma_0}^2}{2D} \tag{3.33}$$

is true, the diffusion coefficient is sufficiently small and therefore the sample diffuses at a rate significantly slower than the velocity that sample is moving in the channel. In this case we can approximate $\sigma(t)$ to equal σ_0 which reduces the equation to:

$$C(x,t) \approx \frac{C_0}{\sqrt{2\pi}\sigma_0} \exp \frac{-(x-vt)^2}{2{\sigma_0}^2} \tag{3.34}$$

suggesting that the concentration profile of the sample would remain constant as it moves down the channel. Work on this area has been started by [14, -0.5in], showing the following information:

As demonstrated in the graphs above, the Gaussian curve is less spread out when D is a small value suggesting this is a good approximation. In the case of a channel with a rectangular cross-sectional area, we have the following relationship [16]:

$$C(x,t) = \frac{C_0}{2}\left[\text{erf}\,\frac{\frac{w_{channel}}{2} - x + vt}{2\sqrt{Dt}} + \text{erf}\,\frac{\frac{w_{channel}}{2} + x - vt}{2\sqrt{Dt}}\right] \tag{3.35}$$

3.3.3 Leakage of Sample Material

One of the challenges facing electrophoretic sample analysis is the fact that after the sample has been injected into separation channel, small amounts of the sample continue to leak into the seperation channel. This is known as sample leakage, and if it is high enough, it can mask the electrophoretic peak that the user is looking for. For the purposes of modeling sample leakage, we can assume an upper bound of the amount of the sample that is leaking into the separation channel as the amount of sample that diffuses into the separation channel from the injection channel. This can be modeled as:

$$C_{intersect}(x,t) = C_0\,\text{erfc}\,\frac{x}{x\sqrt{Dt}} \tag{3.36}$$

Here x, the position across the injection channel, is assumed to be significantly less than the diameter of the separation channel. In order to reduce the amount of sample leakage occurring, a pullback voltage (a voltage difference between the intersection and the ends of the waste/injection channel) is applied. To determine what the concentration of the leaked sample at the position of analysis, we can assume that the sample will move at velocity v down the channel and will have the relationship:

$$C_{intersect}(x,t) = C_0\,\text{erfc}\,\frac{x - vt}{x\sqrt{Dt}} \tag{3.37}$$

3.3.4 Mass Transfer Model

An alternative model for sample leakage is done by analzying the quantity of material left in the waste and injection channels as time varies. Assuming no pullback voltage and an initial analyte concentration of C_0, we get the relationship :

$$m(t) = C_0 A\sqrt{2Dt} \tag{3.38}$$

where m is the amount of mass at time t passing into the cross-section. A is the cross-sectional area of the channel. This relationship can then differentiated and used to determine the amount of sample that has leaked into the separation channel [14]:

$$C_{leak}(t) = \frac{2 \cdot dm}{Av \cdot dt} = \frac{2C_0}{v}\sqrt{\frac{D}{2t}} \tag{3.39}$$

3.3.5 Differentiating Peak from Baseline

The main purpose of these models is to ensure that sample leakage which makes up the baseline or background of the signal does not mask the peak signal that is the main purpose of the electrophoretic circuit. In [14], this is defined as follows:

$$t_{peak} = \frac{x_{detector}}{v} \tag{3.40}$$

where t_{peak} is the time it takes for the sample plug to reach $x_{detector}$ (the location where the sample will be analyzed) when going velocity v. Using one of the models, we can determine:

$$C_{peak} = C(x_{detector}, t_{peak}) \tag{3.41}$$

We can that the max baseline to be:

$$C_{baseline} = kC_{peak} \tag{3.42}$$

where k is significantly less than zero. The k value essentially controls the signal-to-noise ratio that the analysis tool is willing to accept before it can no longer accurately distinguish the signal from background noise.

Chapter 4

Multi-phase Microfluidic Circuits

4.1 Droplet Formation

There are two ways that droplet can be formed. Method one creates water droplets using oil as the solvent. Water is injected from channel two into channel one at a T junction creating water droplets. The droplets are large, occupying most of the channel width and depth as depicted in the figure below.

Figure 4.1: The T-Junction method is one of two methods used for droplet formation.

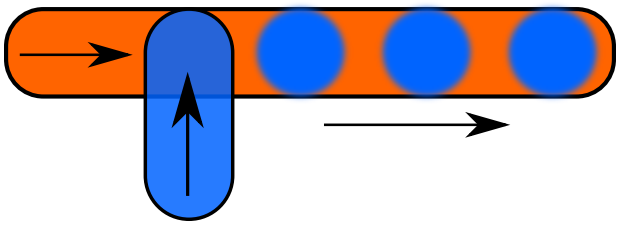

Method two works similarly to method one, as in water is injected into an oil stream however instead of a T junction, a cross junction is used. The oil comes from both side channels as seen in the figure below. Simultaneously, water is injected from centre channel into the cross. Flow of water goes from inside the cross, outwards, creating droplets similar to what is found in method one. The advantage in method two for droplet formation over droplet one is that the droplets produced through method two tend to be more uniform, and therefore has less variance in the statistical distribution of the droplet size.

Figure 4.2: Method two for droplet formation. Water (blue) merges with oil to form water droplets.

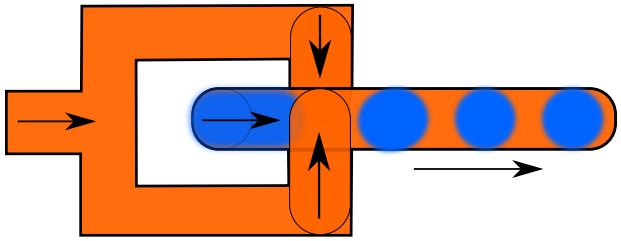

The volume of the droplet can be calculated using using the following equation:

$$V_d = \alpha + \beta \frac{Q_{water}}{Q_{oil}} \tag{4.1}$$

where V_d is the volume of the droplet,α and β are constants determined experimentally and is found in literature, and Q is the flow rate of the respective fluid. Note the frequency or spacing of the droplet is determined from the equation:

$$f = \frac{Q_{water}}{V_d} \tag{4.2}$$

where Q is given by the equation:

$$Q = \frac{\delta P}{R_H} \tag{4.3}$$

where P is the pressure differential from one of the channel to the other and R_H is the hydrodynamic resistance determine by the shape and length of the pipe. Given a cylindrical pipe: .

$$R_H = \frac{8\mu L}{r^4} \tag{4.4}$$

Example of the above relationships in SMT2 format:

```
(assert (= Rh_w (* 8 (* u_w (/ L (^ r 4))))))
(assert (= Rh_o (* 8 (* u_o (/ L (^ r 4))))))
```

```
(assert (= Q_w (/ DP_w Rh_w)))
(assert (= Q_o (/ DP_o Rh_o)))

(assert (= Vd (+ a (* b (/ Q_w Q_o)))))
(assert (= f (/ Q_w Vd)))
```

4.2 Droplet Splitting

The purpose of droplet splitting is to split identical droplets into smaller droplets. Method one uses a T-junction while method two uses a Y-Junction. In method one, the angle of separation between channel two and channel three is 180 degrees, while the angle of separation of channel two and channel three in method two is 90 degrees.

Figure 4.3: T-Junction Droplet Splitting conserves less momentum and is used to separate droplets into different channels

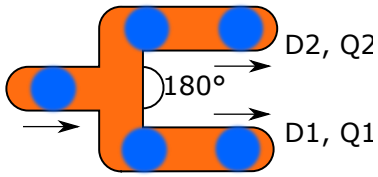

The capillary number is used to determine whether the droplet will split or not. The capillary number C_A is determined by the formula:

$$C_A = \frac{\mu V_{ave}}{\gamma} \tag{4.5}$$

where μ is the viscosity of the solvent (i.e. oil), V_{ave} is the average velocity of the fluid which can be determined using

$$\frac{Q}{A} = V_{ave} \tag{4.6}$$

where A is the cross-sectional area of the channel CH:

Figure 4.4: Y-Junction Droplet Splitting conserves more momentum and is also used to separate droplets into different channels

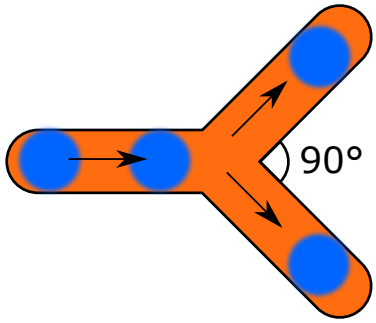

$$A = \frac{CH_{width}}{CH_{depth}} \tag{4.7}$$

and γ is the inter-facial tension between the solvent and the droplet (such as between oil and water). When C_A is larger than the critical droplet number (determined experimentally) of the given channel, the droplet will break. The proportion that the droplet will break is dependent on the flow rates of channel two and channel three. It can be determined by a simple ratio as follows:

$$\frac{Q_1}{Q_2} = \frac{V_{d1}}{V_{d2}} \tag{4.8}$$

where subscript of Q indicates the flow rate of the channel, and V_d indicates the volume of the droplet entering that channel. Method one and method two's varying geometries will result in different critical droplet numbers.

Example of the above relationships in SMT2 format:

```
(assert (= A (/ ChW ChD)))
(assert (= Vave (/ Q A)))
(assert (= Ca (* u (/ Vave gamma))))
(assert (> Ca Crit))
(assert (= (/ Q1 Q2) (/ D1 D2)))
```

Figure 4.5: Increase in channel width reduces spacing between droplets which results in the droplets merging

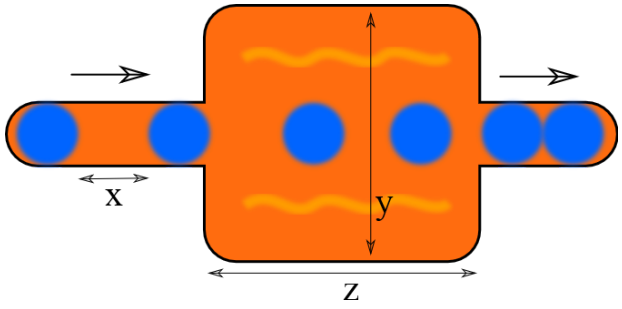

4.3 Droplet Merging

A large channel segment is used to squeeze droplets together and decrease the spacing between them. If spaced far enough, the droplet can merge together to create a continuous fluid and combine contents of the droplet (if the droplet is used as a micro-reactor) [9].

The relationship is as follows:

$$x_c = \alpha + \beta \times K \tag{4.9}$$

where x_c is the location of coalescence (this distance required before the droplets merge), α and β are constants determined experimentally and K is a calculated value determined by:

$$K = \frac{W D_0}{4R^2} \tag{4.10}$$

where D_0 is the distance between the center of one droplet and the other, W is the width of the inlet channel, R is the radius of the droplet when in the large channel segment used for coalescence.

Example of the above relationships in SMT2 format:

```
(assert (= K (/ (* W D0) (* 4 (^ R 2)))))
(assert (= Xc (+ a (* b K))))
```

Figure 4.6: Droplet Traps trap a droplet temporarily for extraction

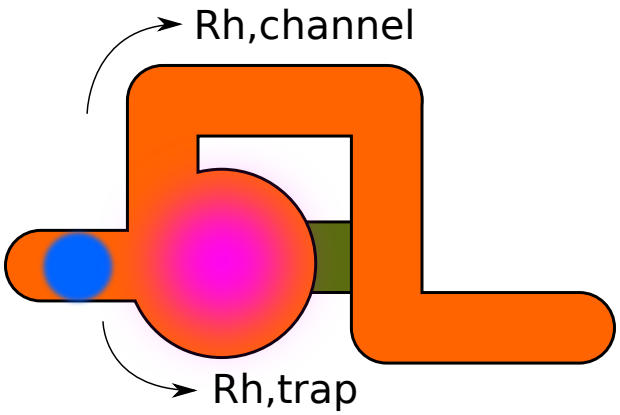

4.4 Trapping Droplets

The droplet trapping is used to extract droplets from the channel. The larger area of the trap results in a smaller hydrodynamic resistance (Ltrap ■ Lchannel, Rtrap ■ Rchannel) which can then forces the droplet into the trap. When occupied, the change in viscosity results in an increase in hydrodynamic resistance, making it greater than the channel, forcing the rest of the droplets to go around the trap. Once the droplet in the channel is removed, again the hydrodynamic resistance of the channel decreases, allowing another droplet to enter the space.

Viscosity of water âĂŞ 0.894, viscosity of oil âĂŞ ranges from 10 âĂŞ 81 mPA.s Note that the viscosity of each section will be based on the ave viscosity (the longer channel will be average of oil + water). Example of the above relationships in SMT2 format:

```
(assert (= Rh_c (* 8 (* u_c (/ L_c (^ r_c 4))))))
(assert (= Rh_x (* 8 (* u_x (/ L_x (^ r_x 4))))))

(assert (= Rh_w (* 8 (* u_w (/ L_t (^ r_t 4))))))
(assert (= Rh_o (* 8 (* u_o (/ L_t (^ r_t 4))))))

(assert (> Rh_c (+ Rh_x Rh_w)))
(assert (< Rh_c (+ Rh_x Rh_o)))
```

- Rh denotes hydrodynamic resistance
- c denotes channel
- x denotes mixed portion of trap
- t denotes uniform portion of trap
- w denotes water
- o denotes oil

Figure 4.7: Droplet mixing can be used to carry out controlled reactions. This droplets are known as Microreactors.

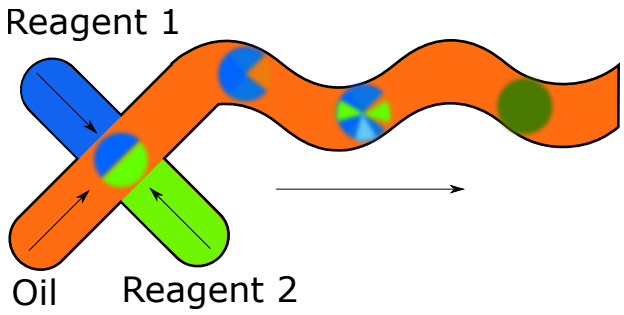

4.5 Mixing Droplets

Two reagents are used in laminar oil flow, both of which are hydrophilic. The bends create tiny vortexes which force the droplet to mix. This requires a numerical simulation method + chemical analysis.

4.6 Sorting

Identical droplets are seperated from each other by having two channels with different R_h. Channel ones R_h increases when occupied, and R_h of channel two decreases when unoccupied and vice versa. Initially, one R_h must be higher than the others to ensure one droplet always enters on direction before the other.

Chapter 5

PDE Reasoning with Error

5.1 Introduction

The purpose of this section is to discuss the velocity profile analysis side of the tool chain. The purpose of analyzing the velocity profile is to determine the shape of the profile and ensure that it is within desired conditions. The purpose of this system is not to complete an accurate simulation, but rather determine solutions that will satisfy the constraints of the model irregardless of the error in the simulation. This is because the problem does not require accuracy, but simply satisfiability. We can therefore simplify the model for the purposes of reducing computational complexity and generate solutions that we know will satisfy the constraints of the problem regardless of the amount of error is introduced due to these simplifications.

5.2 PDE Modeling

Finite Element Method [21] is a method used to numerically approximate the partial differential equations (PDE's) by constructing a mesh. It differs from the Finite Difference Method in that it uses integrals within the node equations. Integrals are not ideally solved using a tool like dReal which was the tool of choice for this research and for this reason the Finite Difference method was used instead.

Model Order Reduction [52] reduces the computational complexity of the problem while retaining most of the behavior of the model. One method used on solving Navier-Stokes

equations is done by reducing the PDEs of a system into a set of ODEs. This is ideal for a lot of microfluidic system's as it does not spatially vary over time. However, this poses a challenge to the toolchain that must prove correctness for multiple microfluidic circuit designs as this method has difficulty discretizing the spatial domain of potential solutions.

Fourier Analysis Method [49] reduces the complexity of the model by using trigonometric functions and reducing the model to a linear one that is not transient. Depending on the problem, transience may be a desirable property and therefore this method may be applied on a case-by-case basis.

5.3 Symmetry

Symmetry in the design of the channels can be exploited to improve the performance times of the system. Experiments were completed by [39] which demonstrated that a 25 inter-dependent equations used to describe a rectangular channel can be reduced through symmetry to less equations. This reduction allowed dReal to terminate within 1.047s while without symmetric manipulation, dReal did not terminate even after 2 hours of execution.

5.4 Mesh Analysis

The accuracy of the numerical approximations of PDE's is dependent on the size of the mesh used for approximating the PDE. The more refined the mesh, the more accurate the simulation. This, however, increases the complexity of the solution and therefore increase the run time. Alternatively, smaller mesh sizes result in faster computations but also larger numerical error.

Figure 5.1: Figure shows how computation time increases as mesh refinement increases [39]

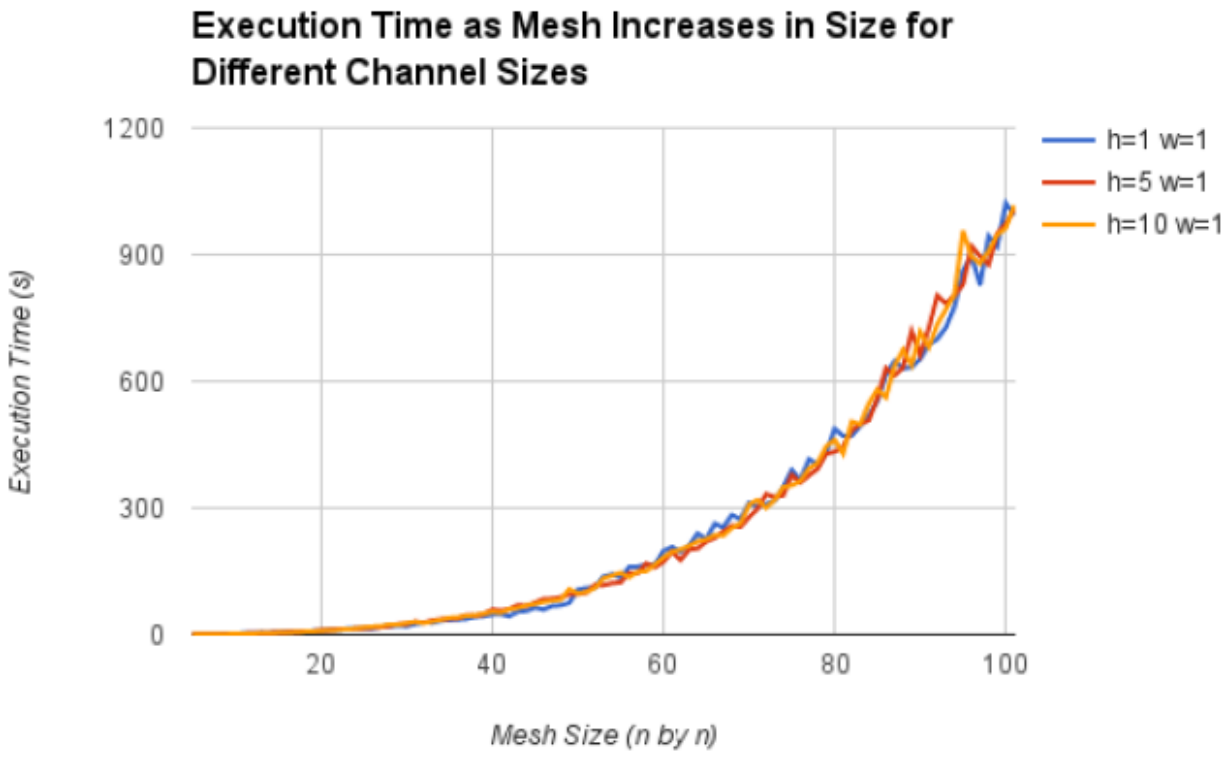

Figure 5.2: Figure shows how the error decreases and mesh refinement increases [39]

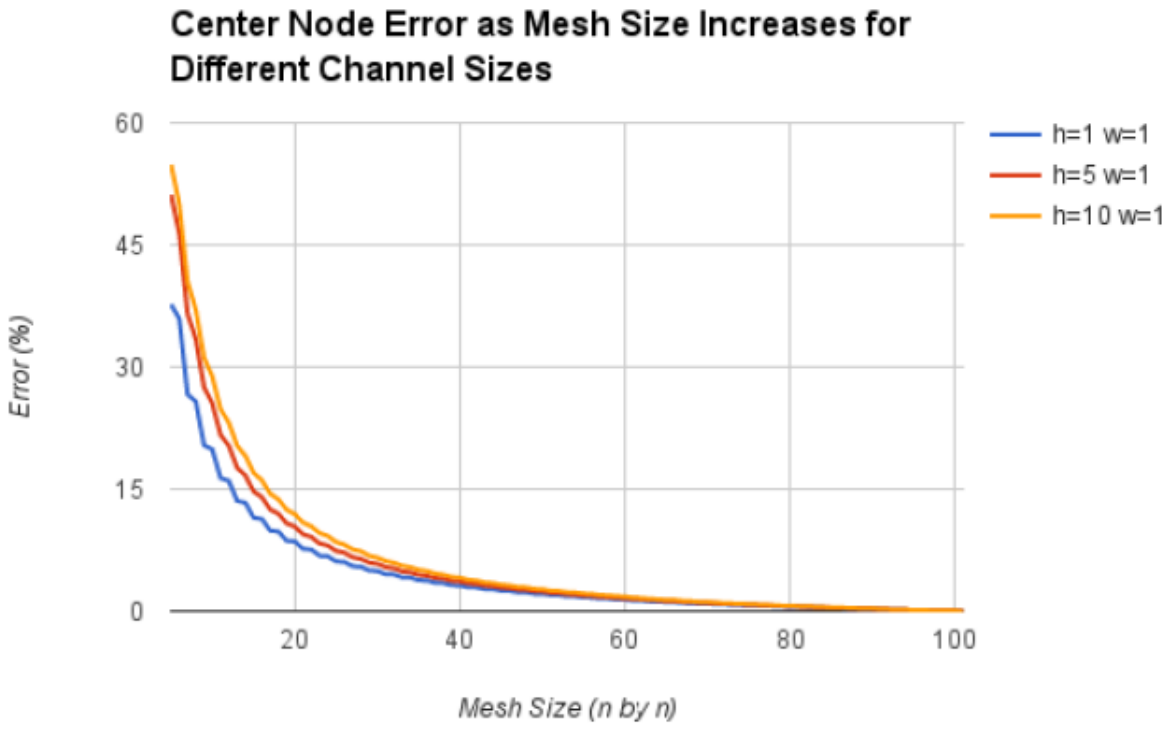

5.5 dReal Analysis

dReal [27] is an SMT solver [20] which reduces non-linear theories over the reals into Boolean Satisfiability (SAT) problems [38]. dReal can determine if a problem is unsatisfiable with certainty, however it cannot determine satisfiability with certainty. The case when it can determine satisfiability without certainty is when the domain is large and it is not computationally feasible for dReal to determine an exact solution. In order to reduce the computational complexity, dReal defines a δ value which determines the precision that dReal will use to search the problem space. The δ value is a representation of the step-size dReal uses when numerically approximating equations. Therefore, unless δ is set to 0, dReal does not determine an exact solution and any solution it determines may still be unsatisfiable.

In experiments conducted by [39], it has been shown that as expected, decreasing the dReal δ value and increasing the number of mesh points increase the accuracy of the system but also the time it takes to compute a solution. [39]. However, due to the δ value, the solution for the solution mesh in the nodes can diverge.

Figure 5.3: Figure shows how the solution in dReal can diverge from Matlab's solution. [39]

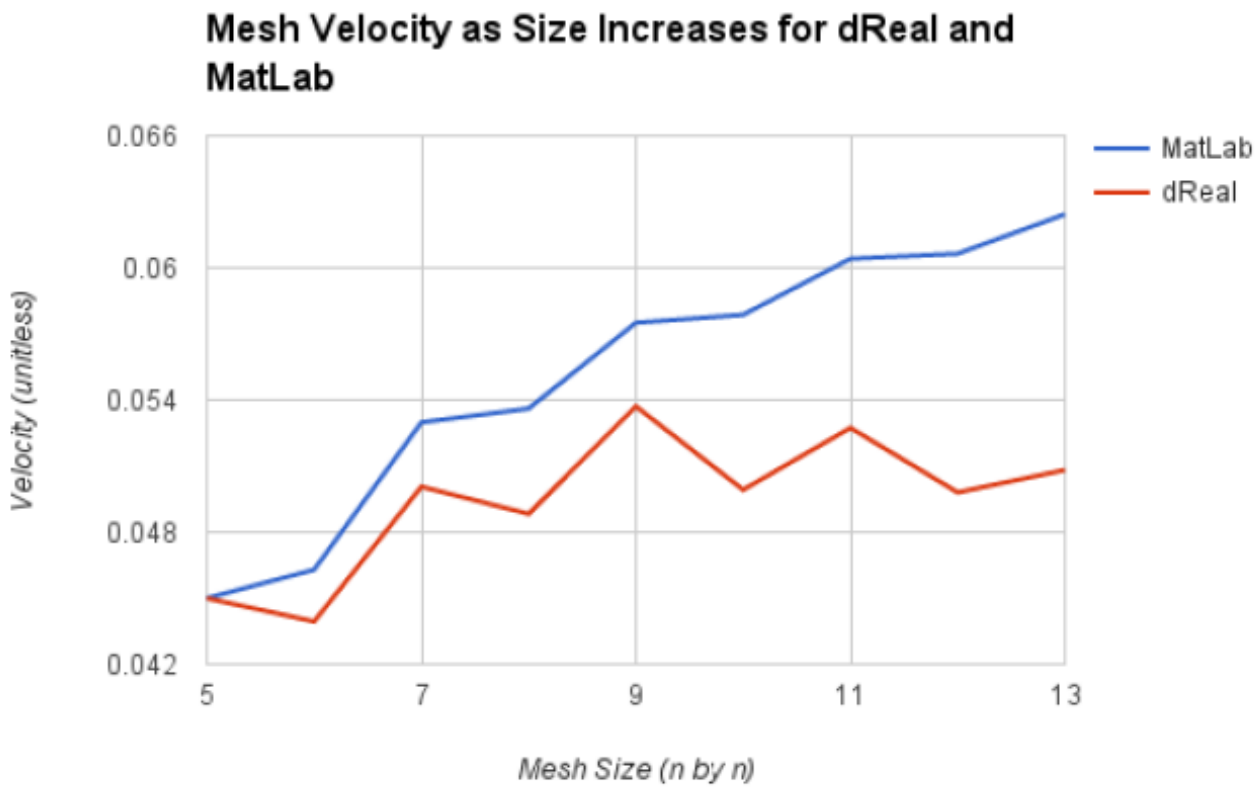

Figure 5.4: Figure shows computation time of Matlab vs dReal for various mesh sizes [39]

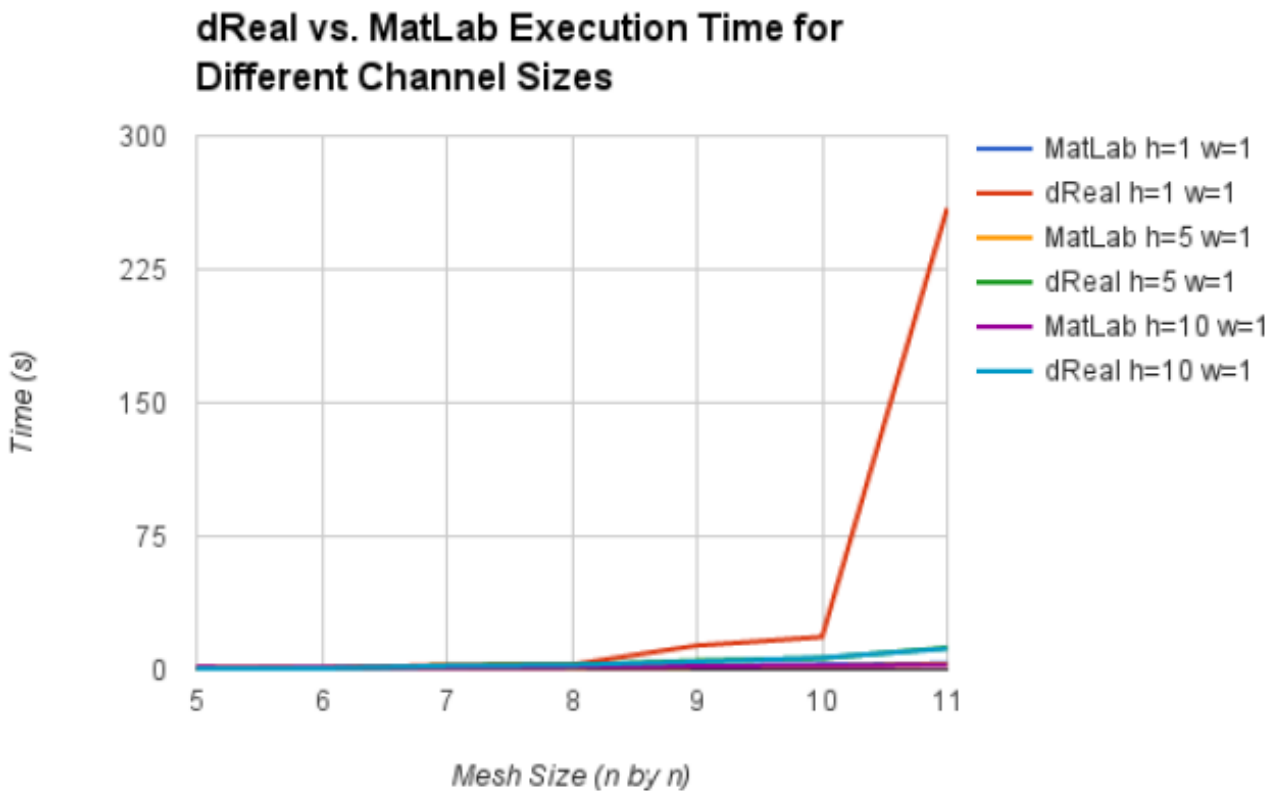

5.6 Error Analysis

dReal needs to use a coarser mesh in order to solve satisfiability problems within a reasonable amount of time. As such, we can determine satisfiable solutions by determining what is the maximum amount error that could exist in the system, and establishing that all solutions must remain below that error interval. There are two sources of error when solving PDE's using dReal; the δ used by dReal and the error in using a coarser mesh.

A proof has been provided by William Lindsay [39] which has determined when using finite difference method along with dReal, the total error in the system is given by:

$$|\tilde{V_{i-1,dReal}}^{j} - \tilde{V_{i-1,exact}}^{j}| = \frac{1}{2}\delta(\frac{\Delta\tilde{x}^2\Delta\tilde{y}^2}{(\frac{h}{w})^2(\Delta\tilde{(y)}^2 + \Delta\tilde{(x)}^2)}) \tag{5.1}$$

5.7 Coarser Mesh Analysis

There are two methods that we consider in order to bound the error in the system and both methods work by assuming that the system is monotonic up till the center of the channel. The first method uses the first derivative of the velocity profile while the second method uses the second derivative of the profile. Below are figures that show the results.

The first derivate velocity profile methods uses the slope between the two corner nodes of the meh to establish the velocity profile. Since the first derivative will always be monotonic towards the center of the channel, we know that it will always predict a center velocity value higher than the true center velocity value. Since in most cases our goal is to ensure that the center velocity is lower than some set value, this is a good way to calculate a satisfiable solution since the true velocity in the center is lower than velocity value calculated through the first derivative method.

The second derivate velocity profile uses slope differences between the first and second nodes (starting from the edge) and the second and third nodes. Again, it is assumed that the second derivative in these cases are at the least monotonic. As it can be seen, especially in the case of the of a more refined mesh (11x11), this method calculates a center mesh velocity that is just barely above the true value of the center of the mesh. This suggests that this method is a good way to calculate the velocity at the center of the mesh that is higher than the true value of the velocity at the center of the mesh. This is perfect for satisfiability problems where the center of the channel's velocity value has a max constraint.

Figure 5.5: Velocity profiles for a 5x5 mesh [39]

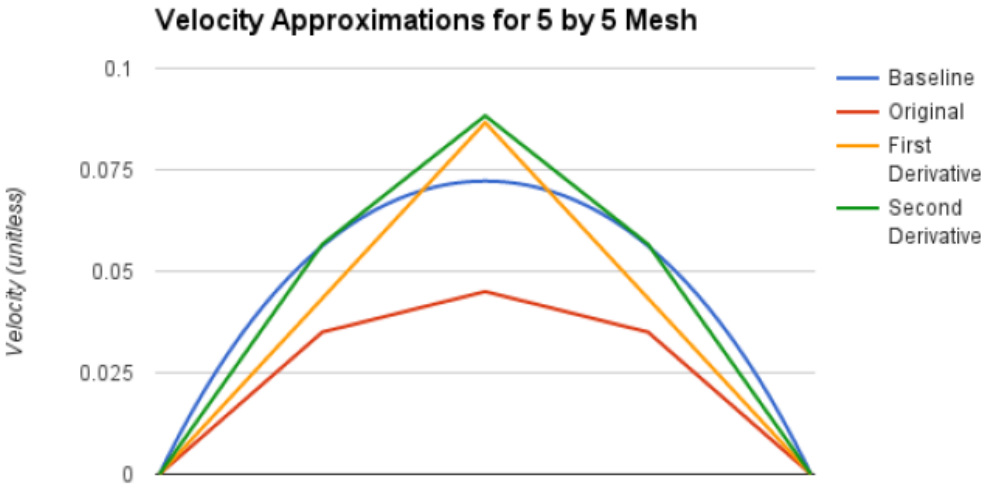

Figure 5.6: Velocity profiles for a 11x11 Mesh [39]

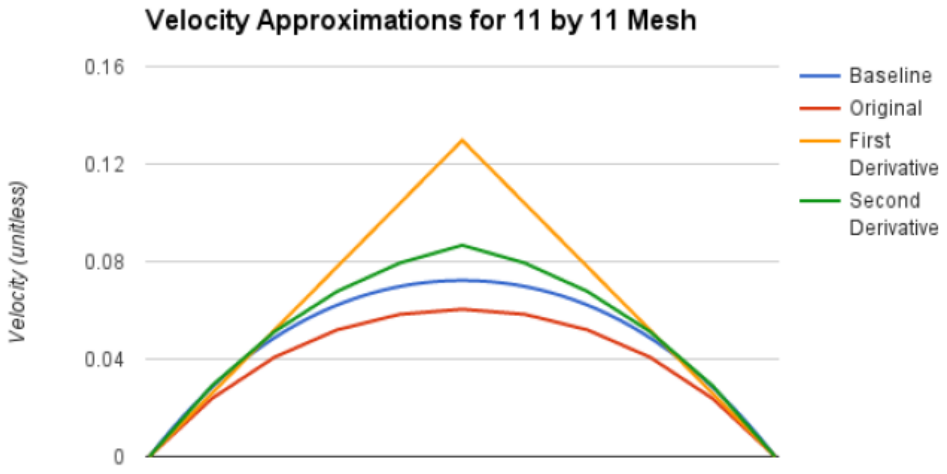

The equation for determining the velocity at the center of the channel using the second derivative method is as follows:

$$\tilde{V_{i,approx}}^{j} = 0.7i\frac{M}{N}((\tilde{V_1}^{j} - \tilde{V_0}^{j}) - (\tilde{V_2}^{j} - \tilde{V_1}^{j})) + \tilde{V_i}^{j} \tag{5.2}$$

For oddly shaped channels, a weighted average method can be applied where mesh points that are closer to the center are given a higher weighting in accuracy than points that are further apart.

5.8 Velocity Profile Constraints

In addition to specifying the volumetric flow rate (Q), the designer might also wish to constrain the velocity profile of the fluid in some channels. In most real channels the velocity profile is non-uniform: due to friction, the fluid closer to the walls of the channel will flow slower than the fluid in the center of the channel. (In fact, we make the common 'no-slip' assumption that the velocity adjacent to the wall is zero.) The volumetric flow rate (Q) is the product of the velocity ($\vec{V}$) and the cross-sectional area of the channel ($\vec{A}$):

$$Q = \int\int_A \vec{V} \cdot \mathrm{d}\vec{A} \tag{5.3}$$

The velocity profile is computed by the Navier-Stokes equation. Under our assumptions of an incompressible Newtonian fluid, laminar flow, no-slip boundaries, and a rectangular channel, the general form of the Navier-Stokes equation reduces to the following:

$$0 = 1 + \left(\frac{h}{w}\right)^2 \frac{\partial^2 \widetilde{V}}{\partial \widetilde{x}^2} + \frac{\partial^2 \widetilde{V}}{\partial \widetilde{y}^2} \tag{5.4}$$

where h and w are the height and width of the pipe respectively, x and y are unitless cross-sectional dimensions, and $\widetilde{V}$ is the unitless expression for velocity. In fluid dynamics, 'unitless' or 'dimensionless' variables are often used; these are obtained as ratios where the units cancel out. We use the tilde-overbar to indicate dimensionless variables.

There is an analogous formulation of Navier-Stokes for cylindrical channels under these assumptions that we do not show here. The dimensionless velocity ($\widetilde{V}$) is related to the velocity (V) according to the following equation:

$$V = \frac{(\Delta P)\, h^2}{\mu L} \widetilde{V} \tag{5.5}$$

where L is the length of the pipe, μ the fluid viscosity and ΔP is the pressure difference between the bracketing nodes of that pipe (all as defined above).

In practice, fluid dynamicists do not solve these differential equations directly but, rather, apply the finite element method to approximate them. This approximation technique used by scientists and engineers is also what brings these equations within the realm of the feasible for solvers such as Z3 and dReal.

Applying the finite element method in this context means dividing up the cross-sectional area of the channel into a mesh and computing the values for each point in the mesh in terms of the adjacent points in the mesh. Consider the point $\langle i, j \rangle$: the velocity at this point will be computed in terms of the velocity at the four surrounding points $\langle i-1, j \rangle$, $\langle i+1, j \rangle$, $\langle i, j-1 \rangle$, and $\langle i, j+1 \rangle$. We write $\widetilde{V}_i^j$ to mean the unitless velocity at point $\langle i, j \rangle$. In the finite element method the Navier-Stokes equation (5.4) becomes:

$$0 = 1 + \frac{\widetilde{V}_{i+1}^j - 2\widetilde{V}_i^j + \widetilde{V}_{i-1}^j}{\Delta \widetilde{x}^2} \left(\frac{h}{w}\right)^2 + \frac{\widetilde{V}_i^{j+1} - 2\widetilde{V}_i^j + \widetilde{V}_i^{j-1}}{\Delta \widetilde{y}^2} \tag{5.6}$$

Finally, we apply the finite element method to the volumetric flow (Q) in equation (5.3) to replace the integrals with summations:

$$Q = \sum_i \sum_j V_i^j \cdot A_i^j \tag{5.7}$$

The microfluidic designer can thusly specify constraints on the velocity profile, such as the maximum permissible velocity or the maximum permissible variance in the velocity, *etc.*

5.9 Energy Constraints

An important relationship that needs to be taken into consideration is the conservation of energy equation. Many of the processes that occur on a microfluidic chip are motivated by heat (such as reactions) and therefore we need to model the heat equations in order

to allow for the user to specify the temperature dependent operating parameters. The conservation of heat equation is as follows:

$$\rho \cdot \hat{C}_p \left(\frac{\partial T}{\partial t} + \nu_x \frac{\partial T}{\partial x} + \nu_y \frac{\partial T}{\partial y} + \nu_z \frac{\partial T}{\partial z} \right) = k \left[\frac{\partial^2 T}{\partial x^2} + \frac{\partial^2 T}{\partial y^2} + \frac{\partial^2 T}{\partial z^2} \right] - \mu \cdot \Phi_v \tag{5.8}$$

where μ, ρ, $\hat{C}_p$ and k are the viscosity, density, heat capacity and thermal conductivity of the fluid, respectively. Φ is used to account for additional energy sources the system may attain. It takes both diffusion and convection into consideration. Using a similar treatment to what was used in approximating the conservation of momentum equation, we can approximate the system using the finite element method as follows:

$$\begin{aligned}
L = &\quad R \\
L = &\quad \rho \cdot \quad \hat{C}_p \quad \left(\tfrac{\widetilde{T}_{i+1}^{j,k,l} + \widetilde{T}_{i-1}^{j,k,l}}{2\Delta t} + \tfrac{\widetilde{T}_{j+1}^{i,k,l} + \widetilde{T}_{j-1}^{i,k,l}}{2\Delta x} + \tfrac{\widetilde{T}_{k+1}^{i,j,l} + \widetilde{T}_{k-1}^{i,j,l}}{2\Delta y} + \tfrac{\widetilde{T}_{l+1}^{i,j,k} + \widetilde{T}_{l-1}^{i,j,k}}{2\Delta z} \right) \\
R = &\quad k \quad [\quad \tfrac{\widetilde{T}(\widetilde{x}_{j+1}, \widetilde{y}_k, \widetilde{z}_l) - 2\widetilde{T}(\widetilde{x}_j, \widetilde{y}_k, \widetilde{z}_l) + \widetilde{T}(\widetilde{x}_{j-1}, \widetilde{y}_k, \widetilde{z}_l)}{\Delta \widetilde{x}^2} + \\
&\qquad\qquad \tfrac{\widetilde{T}(\widetilde{y}_{k+1}, \widetilde{x}_j, \widetilde{z}_l) - 2\widetilde{T}(\widetilde{y}_k, \widetilde{x}_j, \widetilde{z}_l) + \widetilde{T}(\widetilde{y}_{k-1}, \widetilde{x}_j, \widetilde{z}_l)}{\Delta \widetilde{y}^2} + \\
&\qquad\qquad \tfrac{\widetilde{T}(\widetilde{z}_{l+1}, \widetilde{x}_j, \widetilde{y}_k) - 2\widetilde{T}(\widetilde{z}_l, \widetilde{x}_j, \widetilde{y}_k) + \widetilde{T}(\widetilde{z}_{l-1}, \widetilde{x}_j, \widetilde{y}_k)}{\Delta \widetilde{z}^2} \;] - \quad \mu \cdot \Phi
\end{aligned} \tag{5.9}$$

5.9.1 Future Work

Further work needs to be done in developing these models as well as integration with a Counter Example Guided Abstraction Refinement (CEGAR) loop that will enable us to use the information to intelligently explore the solution space.

Chapter 6

Conclusion

There is a tremendous need and opportunity for microfluidic design automation tools [3]. This thesis moves towards this goal broadly in two ways: by identifying specific opportunities within microfluidics, and by identifying the potential applicability of new SMT technology [27] (§5). A solver-based approach to microfluidic design offers the possibility of a correct-by-construction approach, rather than the current build-and-test. Automating design synthesis in this way might also reduce the extensive multi-disciplinary training requirements for those who wish to design microfluidic devices.

The three specific opportunities, and some of the analytic equations required thereof, are: the microhydraulic PinPress (§2, [36]), single-phase electrophoretic cross (§3), and multi-phase T-junction droplet generator (§4). We have started constructing physical prototypes of the PinPress, and it is the basis of a startup company.[1] This company has won a number of awards and grants (§1.3).

There is still tremendous opportunity for future work. Digital circuit design has benefited from over three decades of research in design automation. Microfluidic design automation is just getting started.

[1] Maieutic Enterprises Inc. http://Maieutic.ca

References

[1] Nada Amin, William Thies, and Saman Amarasinghe. Computer-aided design for microfluidic chips based on multilayer soft lithography. In *Proceedings of the 2009 IEEE International Conference on Computer Design*, ICCD'09, pages 2–9. IEEE Press, 2009. ISBN 978-1-4244-5029-9. URL http://dl.acm.org/citation.cfm?id=1792354.1792357.

[2] Mohammed Amini, Mohammed Bakhshi, and Javad Jafari Fesharaki. Design, fabrication, and use of a new reconfigurable discrete die for forming tubular parts. *International Journal for Advanced Manufacturing Technologies*, pages 1055–1063, 2014.

[3] Ismail Emre Araci and Philip Brisk. Recent developments in microfluidic large scale integration. *Current Opinion in Biotechnology*, 25:60–68, 2014.

[4] Supat Arunworradirok and Chanyut Kolitawong. A novel scheme for designing coat-hanger slit dies. In *Commemorative International Conference of the Occasion of the 4th Cycle Anniversary of KMUTT*, 2008.

[5] C.J. Backhouse. *Engineering of Nanobiotechnological Systems*. Gardland Publishing, 2015.

[6] Aditya Bedekar, Yi Wang, Sachin S Siddhaye, Siva Krishnamoorthy, and Stephen F. Malin. Design software for application-specific microfluidic devices. *Clinical chemistry*, 53(11):2023–6, November 2007.

[7] R. Boden, U. Simu, J. Margell, M. Lehto, K. Hjort, G. Thornell, and J.-A. Schweitz. Metallic high-pressue microfluidic pump with active valves. *Solid-State Sensors, Actuators and Microsystems Conference, 2007.*, pages 2429–2432, 2007.

[8] Stephen Boyd, Seung-Jean Kim, Lieven Vandenberghe, and Arash Hassibi. A tutorial on geometric programming. Technical report, Stanford, September 2007.

[9] Nicolas Bremond, Abdou R. Thiam, and Jerome Bibette. Decompressing emulsion droplets favors coalescence. *Physics Review Letters*, pages 1–4, 2008.

[10] R. Bruttomesso, E. Pek, N. Sharygina, and A. Tsitovich. Flexible interpolation with local proof transformation. In *Computer-Aided Design (ICCAD), 2010 IEEE/ACM International Conference*, pages 770–777, 2010.

[11] M. Cayemittes, C. Hankins, and M.R. Tam. An AIDS test that travels well. *IDRC Rep.*, 21:27–28, July 1993.

[12] Krishnendu Chakrabarty and Fei Su. System-level design automation tools for digital microfluidic biochips. In *CODES+ISSS'05*, 2005.

[13] Krishnendu Chakrabarty and Jun Zeng, editors. *Design Automation Methods and Tools for Microfluidics-Based Biochips*. Springer-Verlag, 2006.

[14] Stephen Chou. Systematic design of single-phase microfluidic circuits for electrophoresis. University of Waterloo ECE 499, 2015.

[15] G.E. Collins. Quantifier elimination for real closed fields by cylindrical algebraic decomposition. *Automata Theory and Formal Languages*, pages 134–183, 1975.

[16] J. Crank. *The Mathematics of Diffusion*. Oxford, 1975.

[17] Bernd Ctortecka. High-field nmr in pulsed magnets. *Max-Planck-Innovation GmbH*, page 1, 2008.

[18] R.M.A. Dawson, Z. Shen, and D.A. Furst. The impact of the transient response of organic light emitting diodes on the desing of active matrix oled displays. In *Electron Devices Meeting, 1998. IEDM '98. Technical Digest., International*, 1998.

[19] Leonardo de Moura and Nikolaj Bjørner. Z3: An efficient SMT solver. In *Proc.14th TACAS*, volume 4963 of *LNCS*, pages 337–340, Budapest, March 2008. Springer-Verlag.

[20] deMoura L. Smt solvers: Theory and practice, 2006.

[21] Suli E. *Lecture notes on finite element methods for partial differential equations*. Class Notes, 2012.

[22] electrical4u. Synchronous motor working principle. http://www.electrical4u.com/synchronous-motor-working-principle/, November 2015.

[23] M. K. Ganai and F. Ivancic. Efficient decision procedure for non-linear arithmetic constraints using ordic. In *Formal Methods in Computer-Aided Design*, 2009.

[24] S. Gao, M. Ganai, F. Ivancic, A. Gupta, S. Sankaranarayanan, and E. Clarke. Integrating icp and lra solvers for deciding nonlinear real arithmetic. In *Formal Methods in Computer-Aided Design*, 2010.

[25] Sicun Gao, Jeremy Avigad, and Edmund Clarke. Delta-complete decision procedures for satisfiability over the reals. In *International Joint Conference on Automated Reasoning*, 2012.

[26] Sicun Gao, Jeremy Avigad, and Edmund Clarke. Delta-decidability over the reals. In *Logic in Computer Science*, 2012.

[27] Sicun Gao, Soonho Kong, and Edmund Clarke. dReal: An SMT Solver for Nonlinear Theories of the Reals. In *Proc.Conference on Automated Deduction*, 2013.

[28] N. Gleichmann, P. Horbert, D. Malsch, and T. Henkel. System simulation for microfluidic design automation of lab-on-a-chip devices. In *15th International Conference on Miniaturized Systems for Chemistry and Life Sciences*, Seattle, WA, October 2011.

[29] L. Granvilliers and F. Behamon. Realpaver: an interval solver using constraint satisfaction techniques. *ACM Trans. Math. Softw.*, 32(1):138–156, 2006.

[30] Laura Guerin. The rail gun. http://www.ck12.org/physics/Electromagnetism/rwa/The-Rail-Gun/, November 2015.

[31] Norman Gwangwava, Khumbulani Mpofu, Nkgatho Tlale, and Yan Yu. A methodology for design and reconfiguration of reconfigurable bending press machines (rbpms). *International Journal of Production Research*, pages 6019–6032, 2014.

[32] Takuro Ikeda. *Fundamentals of Piezoelectricity*. Oxford University Press, 1990.

[33] Advanced Cerametrics Inc. 1-3 piezoelectric multilayer composites. *Product Data Sheet*, page 1, 2013.

[34] Andrew B. Kahng, Ion Mandoiu, Sherief Reda, Xu Xu, and Alex Z. Zelikovsky. Evaluation of placement techniques for dna probe layout. In *Computer Aided Design, 2003. ICCAD-2003. International Conference on*, 2003.

[35] H. Kaur, J. Dhanao, and A. Oberoi. An evaluation of rapid kits for dectection of HIV, HBsAg and HCV infections. *Indian J. Med. Sci.*, 67:432–434, July 2000.

[36] Asif Khan, Nemanja Kliska, Nicholas George Vardy, and Alexander Steven Ross. *Polymorphic surface systems and methods*. Patent CA 2,894,983. Canadian Intellectual Property Office, September 3 2015. http://www.ic.gc.ca/opic-cipo/cpd/eng/patent/2894983/summary.html.

[37] A.C. Labbe, D.R. Pillai, B. Hongvangthong, V. Vanisaveth, S. Pomphida, S. Inkathone, D.C. Hay Burgess, and K.C. Kain. The performance and utility of rapid diagnostic assays for plasmodium falciparum malaria in a field setting in the Lao People's Democratic Republic. *Annals of Tropical Medicine and Parasitology*, 95: 671–677, October 2001.

[38] Roychowdhury J. Lee E. and Seshia S. Fundamental algorithms for system modeling, analysis and optimization, 2011.

[39] William Lindsay. Microfluidic velocity profile mesh analysis, 2015.

[40] KJ Magnetics. Temperature and neodymium magnets, 2015.

[41] J. McDaniel, A. Baez, B. Crites, A. Tammewar, and P. Brisk. Design and verification tools for continuous fluid flow-based microfluidic devices. In *18th Asia and South Pacific Design Automation Conference, ASP-DAC*, pages 219–224, Yokohama, Japan, January 2013. IEEE. ISBN 978-1-4673-3029-9. URL http://ieeexplore.ieee.org/xpl/mostRecentIssue.jsp?punumber=6507004.

[42] Allen McDuffee. Navy's new gailgun can hurl a shell over 5,000 mph. *Wired*, page 1, 2014.

[43] J. McFarland and I. R. McNab. A long-range naval railgun. *Magnetics*, pages 289–294, 2003.

[44] W.H. Minhass, P. Pop, and J. Madsen. Synthesis of biochemical applications on flow-based microfluidic biochips using constraint programming. In *Symposium on Design, Test, Integration and Packaging of MEMS/MOEMS (DTIP)*, 2012.

[45] C. Munoz and A. Narkawicz. Fomalization of a representation of bernstein polynomials and applications to global optimization. *Journal of Automated Reasoning*, 2012.

[46] P. Nuzzo, A. Puggelli, S.A. Seshia, and A. L. Sangiovanni-Vincentelli. Calcs: Smt solving for non-linear convex constraints. in r. bloem and n. sharygina. In *Formal Methods in Computer-Aided Design*, pages 71–79, 2010.

[47] S. Ogden, R. Boden, and K. Hjort. A latchable paraffin actuated high-pressue microfluidic valve. *Solid-State Sensors, Actuators and Microsystems Conference, 2009.*, pages 29–32, 2009.

[48] Viorel Paunoiu, Alexandru Epureanu, Dumitru Nicoara, and Ovidiu Ciocan. A review of the sheet metal forming methods using reconfigurable dies. *The Annals Dunarea de Jos University of Galati*, pages 45–50, 2006.

[49] Danchin R. Fourier analysis methods for pdes, 2005.

[50] P.V.M. Rao and Sanjay G. Dhande. A flexible surface tooling for sheet-forming processes: conceptual studies and numerical simulation. *Journal of Materials Processing Technology*, pages 133–143, 2002.

[51] D. Do Rice, Richard G. Duong, editor. *Applied mathematics and modeling for chemical engineers*. John Wiley & Sons, 1995.

[52] Wilhelmus H. Schilders. Introduction to model order reduction. In Wilhelmus H. Schilders, Henk A. van der Vorst, and Joost Rommes, editors, *Model Order Reduction: Theory, Research Aspects and Applications*, volume 13 of *The European Consortium for Mathematics in Industry*, pages 3–32. Springer-Verlag, 2008.

[53] M.F. Schmidt, W.H. Minhass, P. Pop, and J. Madsen. Modeling and simulation framework for flow-based microfluidic biochips. In *Symposium on Design, Test, Integration and Packaging of MEMS/MOEMS (DTIP)*, April 2013.

[54] Neil Sclater. *Mechanisms and Mechanical Devices Sourcebook, 5th Edition*. McGraw-Hill, 2011.

[55] Stanley O. Starr, Rober C. Youngquist, and Robert B. Cox. A low voltage railgun. *American Journal of Physics*, pages 38–43, 2013.

[56] T. Thorsen, S. J. Maerki, and S. R. Quake. Microfluidic large-scale integration. *Science*, 298(5593):580–584, October 2002.

[57] M.L. Trouwborst, S. J. van der Molen, and B. J. van Wees. The role of joule heating in the formation of nanogaps by electromigration. *Journal of Applied Physics*, pages 1–8, 2005.

[58] Daniel Walcyzk and Chris Munro. Reconfigurable pin-type tooling: A survey of prior art and reduction to practice. *Journal of Manufacturing Science and Engieering*, pages 551–565, 2007.

[59] Zhijian Wang. *Rapid Manufacturing of Vacuum Forming Components Utilising Reconfigurable Screw Pin Tooling*. University of Nottingham, 2010.

[60] Wikipedia. Finite strain theory. https://en.wikipedia.org/wiki/Finite_strain_theory, 2015.

[61] Wikipedia. Joule heating. https://en.wikipedia.org/wiki/Joule_heating, 2015.

[62] Wikipedia. Lorrentz force. https://en.wikipedia.org/wiki/Lorentz_force, 2015.

[63] Wikipedia. Buckling. https://en.wikipedia.org/wiki/Buckling, 2015.

[64] Wikipedia. Mooney-Rivlin solid. https://en.wikipedia.org/wiki/Mooney-Rivlin_solid, 2015.

[65] Dapeng Wu, Jianhua Qin, and Bingcheng Lin. Electrophoretic seperations on microfluidic chips. *Journal of Chromatography A*, 1184:542–559, December 2008.

[66] Paul Yager, Thayne Edwards, Elain Fu, Kristen Helton, Kjell Nelson, Milton R. Tarm, and Bernhard H. Weigl. Microfluidic diagnostic technologies for global public health. *Nature*, 442:412–419, July 2006.

[67] J.B. Zhang, X.H. Li, F. Ning, and X.S. Guo. Relationship between expression GYPC and TRIP3 genes and prognosis of acute lymphoblastic leukemia in children. *Zhongguo Dang Dai Er Ke Za Zhi*, 11:29–32, January 2009.

[68] B.G. Zhukov, R.O. Kurakin, V.A. Sakharov, S.V. Bobashev, S.A. Ponyaev, B.I. Reznikov, and S.T. Rozov. A compact railgun accelerator for millimeter-sized dielectric solid armatures. *Ioffe Physical Technical Institute*, pages 570–573, 2013.